Biotechnology Reports 36 (2022) e00775

Contents lists available at ScienceDirect

Biotechnology Reports

journal homepage: www.elsevier.com/locate/btre

Research Article

Comparative computational study to augment UbiA prenyltransferases inherent in purple photosynthetic bacteria cultured from mangrove microbial mats in Qatar for coenzyme Q_{10} biosynthesis.

Drishya M. George [a,1], Ramya Ramadoss [b,1], Hamish R. Mackey [a,c,2], Annette S. Vincent [b,*]

[a] College of Health and Life Sciences, Hamad bin Khalifa University, Qatar Foundation, Doha, Qatar
[b] Biological Sciences, Carnegie Mellon University Qatar, Doha, Qatar
[c] Division of Sustainable Development, College of Science and Engineering, Hamad bin Khalifa University, Qatar Foundation, Doha, Qatar

ARTICLE INFO

Keywords:
Anoxygenic phototrophic bacteria (APB)
Resource recovery
Purple photosynthetic bacteria (PPB)
Coenzyme Q10 (CoQ_{10})
Protein modeling
Multiple ligand simultaneous docking (MLSD)

ABSTRACT

Coenzyme Q_{10} (CoQ_{10}) is a powerful antioxidant with a myriad of applications in healthcare and cosmetic industries. The most effective route of CoQ_{10} production is microbial biosynthesis. In this study, four CoQ_{10} biosynthesizing purple photosynthetic bacteria: *Rhodobacter blasticus, Rhodovulum adriaticum, Afifella pfennigii* and *Rhodovulum marinum*, were identified using 16S rRNA sequencing of enriched microbial mat samples obtained from Purple Island mangroves (Qatar). The membrane bound enzyme 4-hydroxybenzoate octaprenyltransferase (UbiA) is pivotal for bacterial biosynthesis of CoQ_{10}. The identified bacteria could be inducted as efficient industrial bio-synthesizers of CoQ_{10} by engineering their UbiA enzymes. Therefore, the mutation sites and substitution residues for potential functional enhancement were determined by comparative computational study. Two mutation sites were identified within the two conserved Asp-rich motifs, and the effect of proposed mutations in substrate binding affinity of the UbiA enzymes was assessed using multiple ligand simultaneous docking (MLSD) studies, as a groundwork for experimental studies.

List of abbreviations

APB	Anoxygenic phototrophic bacteria
PHA	Poly-β-hydroxyalkanoate
SCP	Single cell protein
CoQ_{10}	Coenzyme Q10
PPB	Purple photosynthetic bacteria
PNSB	Purple non-sulfur bacteria
PSB	Purple sulfur bacteria
MEP	Methylerythritol phosphate pathway
UbiA	4-hydroxybenzoate octaprenyltransferase
PHBA	p-Hydroxybenzoic acid or 4-hydroxybenzoic acid
FACS	Fluorescence activated cell sorting
QIIME 2	Quantitative insights into microbial ecology 2
GSPP	Geranyl s-thiolodiphosphate
RCSB	Research Collaboratory for structural bioinformatics
PDB	Protein data bank
MLSD	Multiple ligand simultaneous docking
RMSD	Root Mean Square Deviation

1. Introduction

Since the start of the COVID-19 pandemic there has been a paradigm shift in consumer habits with an increased focus on leading a healthy lifestyle. Consequently, this has propelled the sales of nutraceuticals such as CoQ_{10} [1]. Research reports have projected a 10.5% compounded annual growth rate (CAGR) for this compound from 2021–2027, which will lead to a market revenue of over $1.15 billion by 2027 [2,3]. Currently, this compound, owing to its antioxidant properties, is a popular active ingredient in several cosmetic skin care formulations and dietary supplements [4–6]. In human beings CoQ_{10} functions as a powerful antioxidant, protecting lipids and lipoprotein from oxidation [7]. It is also involved in the oxidation of sulfide [8], regulation of the mitochondrial permeability transition pore and in the transfer

* Corresponding author.
E-mail address: annettev@andrew.cmu.edu (A.S. Vincent).
[1] These authors contributed equally to this work.
[2] Department of Civil and Natural Resource Engineering, University of Canterbury, Christchurch, New Zealand

https://doi.org/10.1016/j.btre.2022.e00775
Received 3 August 2022; Received in revised form 31 October 2022; Accepted 11 November 2022
Available online 12 November 2022

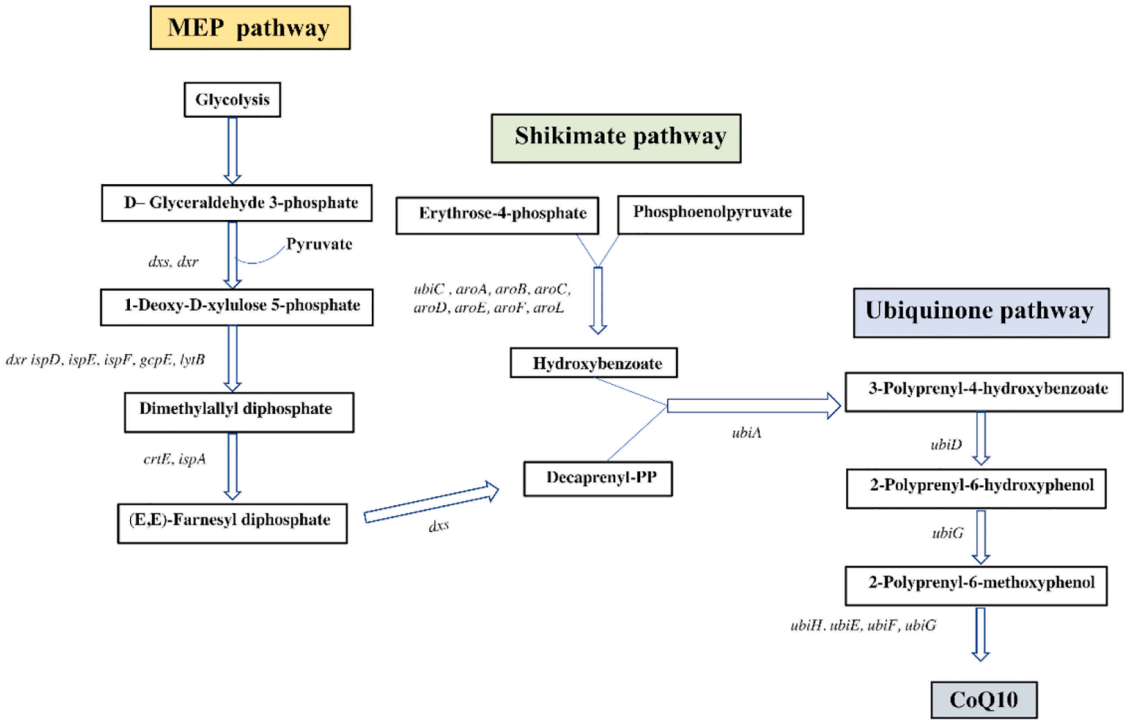

Fig. 1. . Biosynthetic pathway of CoQ_{10} synthesis in the purple non-sulfur bacteria, *R. sphaeroides,* adapted from Li et al. [34].

of Ca^{2+} and other ions across biological membranes [9]. CoQ_{10} deficiencies in humans have resulted in several metabolic, cardiovascular, and central nervous system disorders [10–13].

The production of CoQ_{10} can either be via a chemical or a microbial route. The chemical synthesis of this compound is normally associated with expensive substrates, absence of stereoselectivity, and production of large amounts of chemical waste, thus the preferred route is microbial biosynthesis [14,15]. Prokaryotic native producers of CoQ_{10} include *Agrobacterium tumefaciens, Paracoccus denitrificans* and *Protomonas extorquens* [16,17]. *Rhodopseudomonas palustris, Rhodospirillum salexigens, Rhodobacter capsulatus* and *Rhodobacter sphaeroides* are purple photosynthetic bacteria, a division of anoxygenic phototrophic bacteria, which have also been identified as native CoQ10 producers[18]..

Purple photosynthetic bacteria, especially, purple non-sulfur bacteria (PNSB) have been well characterized and studied for wastewater-based resource recovery. Low energy requirements, use of varied metabolic routes, and cost effectiveness associated with growth and maintenance of these organisms are some of the advantages associated with utilizing these bacteria for resource recovery purposes. There have been several extensive reviews that have elucidated the various environmental biotechnology applications of these bacteria including bioremediation [19,20], resource recovery and synthesis of value-added products [21–23]. Poly-β-hydroxyalkanoates (PHAs) [24], single cell protein (SCP) [25], biofertilizers [26], carotenoid pigments [27], bacteriochlorophyll [28], and CoQ_{10} [29]are some of the value-added compounds that can be synthesized by purple photosynthetic bacteria. Among these compounds, CoQ_{10} is a high value product with a market price of over $400/kg [30], which is greater than that of most other value-added products generated by these bacteria [21]. Mangrove ecosystems are unique ecological niches that are rich in soluble organic matter and characterized by recurrent tidal flooding which in turn results in different pH, light, salinity, and nutrient gradients making it a very conducive habitat for APB, particularly PNSB [31,32]. PNSB genera common to mangrove ecosystems include *Afifella, Rhodobium, Rhodovulum, Rhodovibrio, Roseospira, Rhodobacter* and *Rhodothalassium* [27]. Given the advantageous culturing conditions and indigeneity, this study aims to propound PNSBs isolated from the microbial mat samples of Purple Island Mangroves, Qatar as efficient industrial bio-synthesizers of CoQ_{10}.

In purple photosynthetic bacteria, the biosynthesis of CoQ_{10} comprises of 3 pathways [33,34] – (i) methylerythritol phosphate (MEP) pathway; (ii) the shikimate pathway and (iii) ubiquinone modification pathway. One of the key enzymes involved in the synthesis of CoQ_{10} is the prenyltransferase enzyme, UbiA. This enzyme is involved in the transfer of the 10-isoprenoid tail generated from the MEP pathway to the benzoquinone nucleus synthesized from the shikimate pathway [33]. Subsequently, the compound undergoes hydroxylation, methylation, and decarboxylation to form CoQ_{10} [33,35,36]. The ubiquinone biosynthetic pathway along with the key enzymes involved in its biosynthesis are outlined in **Fig. 1**. Certain structural features of the UbiA enzyme enable it to incorporate prenyl diphosphates of different lengths, which in turn governs the type of coenzyme ($CoQ_{6–10}$) produced [37]. While this enzyme lacks specificity with regards to the length of the isoprenyl substrate [38], it is highly specific to the p-hydroxybenzoic acid (PHBA) substrate [39].

Deoxyxylulose 5-phosphate synthase (*dxs*), deoxyxylulose 5-phosphate reductoisomerase (*dxr*), 2-C-Methyl-D-erythritol-4-phosphatecytidyltransferase (*ispD*), 4-diphosphocytidyl-2-C-methyl- D-erythritol kinase (*ispE*), 2-C-Methyl-D-erythritol 2,4-cyclodiphosphate synthase (*ispF*), (E)-4-Hydroxy-3-methyl-but-2-enyl pyrophosphate (HMB-PP) synthase (*GcpE*), (E)-4-Hydroxy-3-methyl-but-2-enyl pyrophosphate (HMB-PP) reductase (*lytB*), farnesyl diphosphate synthase (*ispA*), geranylgeranyl diphosphate (GGPP) synthase (*crtE*), decaprenyl diphosphate synthase (*dps*), chorismate pyruvate-lyase (*ubiC*), 5-enolpyruvoylshikimate-3- phosphate (EPSP) synthase (*aroA*), 3-dehydroquinate synthase (*aroB*), Chorismate synthase (*aroC*), 3-dehydroquinate dehydratase (*aroD*), shikimate dehydrogenase (*aroE*), 3-deoxy-D-arabino-heptulosonate 7-phosphate (DAHP) synthase (*aroF*), shikimate kinase (*aroL*), 4-hydroxybenzoate octaprenyltransferase (*ubiA*), 3-octaprenyl-4-hydroxybenzoate carboxy-lyase (*ubiD*), ubiquinone biosynthesis O-methyltransferase (*ubiG*), 2-octaprenyl-6-methoxyphenol hydroxylase (*ubiH*), ubiquinone/menaquinone biosynthesis C-methyltransferase (*ubiE*) and 3-demethoxyubiquinol 3-hydroxylase (*ubiF*).

A recent study by Xu et al. [40], has identified UbiA as one of the rate

limiting enzymes in CoQ_{10} biosynthesis. The overexpression of this enzyme along with decaprenyl diphosphate synthase (DPS) and 1-deoxy-xylulose-5-phosphate synthase (DXS) led to 2.9-fold increase in CoQ_{10} synthesis in *R. palustris*. The first X-ray crystal structure of the UbiA homolog belonging to *Aeropyrum pernix* was characterized by Cheng and Li [41]. The protein is comprised of nine transmembrane helices arranged in a U shape surrounding a large central cavity which forms a transmembrane domain with extramembrane cap domain atop. The cap domain encompasses two conserved Asp-rich motifs, $D_{XXX}D$ and $Y_{XXX}D$. These conserved motifs protrude into the central cavity and are involved in substrate binding via polar interactions, vital for the catalytic function of the enzyme [42]. Hydrophobic residues lining the central cavity are inferred to accommodate the isoprenyl chain, while a pocket lined with basic residues interacts with the aromatic substrate. On one side of the central cavity is an opening called the lateral portal that could plausibly act as a channel for product release [42]. Corresponding motifs have been identified in members of the UbiA superfamily including: COQ2, UBIAD1, and MenA [42].

Enzymes are the biocatalysts extensively used for various biotechnological applications pertaining to their numerous advantages over chemical catalysts. Industrial bioprocesses often require enzymes with improved catalytic efficiency and stability. The desired functionalities in an enzyme can be achieved by protein engineering strategies like site-directed mutagenesis and directed evolution. Unlike the directed evolution method and the random site-directed mutagenesis method which require extensive resources, rational site-directed mutagenesis based on sequence and structure of an enzyme is a straightforward efficient approach for protein engineering [43]. This involves analyzing the three-dimensional protein structure and identifying plausible point mutation sites in its catalytic cavity [44]. Further, designation of the right amino acid residue for substitution at the mutation site is guided by the natural diversity of the enzyme's catalytic cavity [45].

Rational protein engineering for enhanced functionality of enzymes for industrial applications is greatly revolutionized with the advent of various computational tools for protein modeling, protein sequence/structure comparison, bioinformatic protein databases and molecular docking [43]. Li et al. [46] have highlighted the role of computational enzyme design in providing the necessary information regarding de novo enzyme design. They have demonstrated the role of this approach in enhancing the activity and stability of the enzyme in a more effectual manner. Investigations by Ramadoss et al. [47] have demonstrated the importance of comparative computational analysis methods in characterizing endolysins, inherent to novel bacteriophages which could be used as 'enzybiotics'. A more recent study by Contractor et al. [48] utilized computational tools to investigate the effect of mutations in the receptor binding domain of Delta and the Omicron variants, on its binding to neutralizing antibodies. They emphasized that in silico studies were a rapid and cost-effective approach that could lay the foundation for efficient vaccine design.

The present study aims to (i) enrich PNSB from the mangrove microbial mats using different culturing conditions, (ii) determine plausible mutation sites and substitution residues to enhance the functional efficiency of the UbiA enzymes inherent in the identified bacteria by comparative computational study and (iii) assess enhanced substrate reactivity of the UbiA enzymes using MLSD studies. This study is a preliminary *in silico* assessment to set the necessary precedents for future laboratory investigations. To our knowledge, this is the first computational study to investigate protein engineering strategies for enhancement of the functional efficiency of UbiA enzyme present in purple photosynthetic bacteria.

2. Methodology

2.1. Developing cultures from isolated microbial mats

A recent experiment in our lab focused on the enrichment of anoxygenic phototrophic bacteria, particularly purple photosynthetic bacteria from microbial mats isolated from a mangrove ecosystem based in Qatar. This included using Nile red dye to stain PHA inclusions present in the bacteria within the cultures, and then sorting these cells using fluorescent activated cell sorting (FACS) to obtain a more enriched culture of APB. Cells that were obtained post FACS were grown under two specified IR light conditions, low IR light at 850 nm and high IR light at 940 nm and were designated as enriched low IR (EL), enriched high IR (EH), while the original pre-FACS cultures were designated as mixed low IR (ML) and mixed high IR (MH) cultures (refer **Fig. S1**). These cultures were then further assessed for the synthesis of different value-added compounds generated by purple photosynthetic bacteria. From this study we were able to identify four PNSBs, which we would like to further examine for their ability to synthesize CoQ10.

2.2. 16S rRNA sequencing

2.2.1. RNA/DNA isolation and sequencing

A fixed volume (5–10 ml) of each culture obtained on Day 18 (endogenous phase), was filtered through a 0.22 μm sterilized Durapore® membrane filter paper (MilliporeSigma, USA) and stored at -80 °C until analysis. The RNA/DNA were isolated, according to the manufacturer's protocol, from each sample using the RNeasy PowerWater® Kit and DNeasy PowerWater® Kit (Qiagen, Hilden, Germany), respectively. cDNA conversion of isolated RNA samples was performed using the ProtoScript® II First Strand cDNA Synthesis Kit (New England Biolabs, USA) where 1 μL each of both, the random primer mix and the oligo-dT were added to the samples. After DNA extraction and cDNA conversion (for isolated RNA), a Qubit Fluorometer (Life Technologies, UK) was used to determine the concentration of the samples, followed by PCR amplification of the V3-V4 hypervariable region of the 16SrRNA from the isolated samples (DNA and RNA) using MiSeq Reagent Kit v3 (600 cycle) catalog # MS-102-3003 (Illumina, Inc., USA) according to the manufacturers protocol. A (2%) agarose gel electrophoresis was run to extract the PCR products followed by purification of the amplicons and ligation of Illumina adapters. Once the samples were sequenced using the Illumina platform, the resultant paired-end reads were processed using the quantitative insights into microbial ecology 2 (QIIME 2) bioinformatics tool [49,50].

2.2.2. Bioinformatics analysis

QIIME 2 analysis [49] was performed on the raw data deposited in the sequence read archive (SRA) under the SRA accession numbers SAMN29969433, SAMN29969432, SAMN29969431, SAMN29969430, SAMN29969429 and SAMN29969428, as a part of BioProject number PRJNA862337. The paired-end sequence data obtained from the MiSeq platform was imported to the QIIME 2 (version 2021.4) pipeline and demultiplexed using q2-demux plugin followed by quality filtering using DADA2 (q2-dada2 plugin) [51]. Classify-sklearn naïve Bayes taxonomy classifier in the q2-feature-classifier [52] was trained using the reference sequences from SILVA SSU rRNA gene database [53–55] to assign taxonomy of the amplicon sequence variants (ASVs). The alpha-diversity metrics (Shannon's Diversity) and beta-diversity metrics (Bray-Curtis dissimilarity) were estimated using the q2-diversity plugin after samples were rarefied with a sampling depth of to 4450 and 1000 sequences per sample, respectively.

2.3. Estimation of CoQ_{10}

The CoQ_{10}estimation required an initial step of bacteria cell disruption, as described in Zhang et al. [56], to extract the compound. A CoQ_{10} analytical standard (Sigma-Aldrich USA) was used to generate a standard curve. The amount of CoQ_{10} present in the cultures was estimated using the Agilent Poroshell 120 EC—C18 (100mmx 3.0 mm x 2.3um) (Agilent Technologies, USA) HPLC with a mobile phase of 65% methanol and 35% ethanol. The flow rate was set at 1.5 ml/min, and a

Table 1
UbiA enzymes. List of protein IDs corresponding to the UbiA enzymes belonging to the different bacteria utilized in this study.

UbiA enzyme ID	**Source Organism**
Candidate Organisms	
PTE13960.1	*Rhodobacter blasticus*
WP_132,604,782.1	*Rhodovulum adriaticum*
WP_051631208.1	*Afifella pfennigii* DSM 17,143
WP_132,460,628.1	*Rhodovulum marinum*
Native/ Industrial Producers	
ACE99883.1	*Rhodopseudomonas palustris* TIE-1
WP_011746970.1	*Paracoccus denitrificans* ATCC 19,367
WP_099085631.1	*Agrobacterium tumefaciens* BIM B-1315G
AEO77955.1	*Pseudomonas aeruginosa* M1
WP_060836425.1	*Rhodovulum sulfidophilum* DSM 2351
Q9YBM8	*Aeropyrum pernix* K1

wavelength of 275 nm was used for the detection of CoQ_{10}. The dry cell weight of the compound was estimated using (**Eq. (1)**).

$$CoQ_{10/TSS} = CoQ_{10/ext} \times \frac{V_{ext}}{V_{cult}} \times \frac{1}{C_{TSS/L}} \quad (1)$$

$CoQ_{10/ext}$ = *estimated* $CoQ10$ *from extract*; V_{ext} = *volume of extract*; V_{cult} = *volume of the culture and*

$C_{TSS/L}$ = *total suspended solids* (*TSS*) *value for a fixed volume ofthe culture*

2.4. Gathering sequence information of UbiA and identification of mutation sites

The substrate bound UbiA from *A. pernix* K1 is well characterized [41] and the X-ray crystallographic 3-dimensional structure is deposited in protein data bank (PDB) under the accession code - 4OD5. The protein sequences of UbiA enzyme and 4-hydroxybenzoate octaprenyl transferase, belonging to the identified purple photosynthetic bacteria and native/industrial producers of CoQ_{10} were fetched from NCBI, and the enzyme details were confirmed from UniProt. The accession number of the UbiA enzyme sequences for all the bacteria used in this study are summarized in **Table 1**.

UbiA of *A. pernix* K1, was reported to contain three conserved motifs that protruded in the central cavity facilitating substrate binding [41]. To identify the corresponding conserved substrate binding pocket inherent in the protein sequences of candidate organisms mentioned in **Table 1.**, multiple sequence alignment was done using MUltiple Sequence Comparison by Log- Expectation (MUSCLE) tool [57]. Further, prospective residues that were prevalent in UbiA of native/industrial bacteria, but vary from UbiA of candidate organisms, were designated as mutational sites.

Potential phosphorylation sites in protein sequences were determined using the GPS server [58,59]. This server uses a group-based phosphorylation scoring (GPS) method to predict kinase-specific phosphorylation sites. The Phobius webserver [60] was used to deduce the transmembrane topology of the protein sequences and Protter web-tool [61] was used to visualize the same.

2.5. Extended motif discovery by protein sequence cluster analysis of 4-hydroxybenzoate octaprenyl transferase

The UniProt [62] protein database (accessed January 2022) was queried using the search term "4-hydroxybenzoate octaprenyl transferase". Only the entries annotated as 4-hydroxybenzoate octaprenyl transferase were selected, post removal of those annotated with the term "Probable" or "Putative" and those with length of protein sequence shorter than 200 base pairs (refer **Table S1**). The resulting protein sequence dataset was subjected to sensitive protein sequence searching using the MMseqs2 tool [63] with varied parameters to identify the lone cluster of similar sequences that included most of the sequences listed in Methodology Section 2.4. This was followed by the discovery of un-gapped motifs using the MAST tool [64] in MEME online suite [65].

2.6. Docking studies

2.6.1. Ligand preparation

To study the putative enzyme-substrate binding interactions, the substrates: p-hydroxybenzoic acid (PHBA) and geranyl s-thiolodiphosphate (GSPP) bound to the UbiA enzyme in PDB ID: 4OD5, were extracted and subsequently used for docking analysis with the modelled structures of wild-type and mutated enzymes listed in **Table 1**.

2.6.2. Protein modeling

Three-dimensional structure of the UbiA enzyme sequences listed in **Table 1.** was predicted using Iterative Threading ASSEmbly Refinement (I-TASSER) [66–68] protein modeling server with default settings. The model with the best c-score was selected. This is a confidence score that assesses the quality of the models predicted by I-TASSER and is estimated based on the significance of threading template alignments along with the convergence parameters of the simulations of structural assembly. The range of the c-score is typically between -5 and 2; the higher the c-score value, the higher the confidence level in the predicted structure. Adding to it, the model quality was also assessed using PROCHECK [69] and ProSA [70] tools (refer **Fig. S2-S3**). The model with the highest c-score was protonated, and Kollman charges were added to the model using the Dock Prep tool inherent in UCSF Chimera [71].

2.6.3. Multiple ligand simultaneous docking studies

As a first step, docking studies were performed using each of the modelled and protonated UbiA enzymes listed in **Table. 1.** as receptors and PHBA as ligands, using MTiAutodock 4.2.6. webserver [72] in blind docking mode. In addition to the docked enzyme-ligand complex, details regarding the top 10 ligand poses with their corresponding docking score, ranked in descending order (best to poor) were generated [72]. The output file of the docked structure is in pdbqt format and was visualized using PyMOL [73]. The ligand pose bound to the vicinity of conserved binding pocket of the enzyme and had the best docking score, was identified, and analyzed for ligand interacting residues using PDBsum tool [74–76].

In the second docking step, the selected UbiA enzyme-PHBA bound complex was used as the receptor and GSPP as ligand in MTiAutodock 4.2.6. webserver, followed by identification of interacting residues in PDBsum tool. The docked complex with GSPP bound at the vicinity of PHBA was designated as the final protein-ligand complex.

Likewise, PHBA followed by GSPP ligand simultaneous docking was carried out with each of the mutated UbiA enzymes as receptor to analyze the effect of point mutation on substrate binding affinity. Comparative analysis of docking scores of final protein-ligand complexes derived from the antecedent and mutated candidate UbiA enzymes was done to identify propitious mutants with improved substrate reactivity. All the enzyme-ligand complexes were visualized using PyMOL (Schrödinger, LLC) visualization software and their surface coloring based on electrostatic potential was done using ChimeraX [71].

3. Results and discussion

3.1. 16S metagenomics and QIIME 2 analysis

Due to the non-specific nature of Nile red, this stain tends to bind to other lipid inclusions and cell envelopes apart from PHA granules [77–79]. Additionally, since heterotrophic bacteria are also proficient producers of PHA [80–82] a large proportion of non-phototrophic bacteria were also selected during the FACS procedure and constituted the

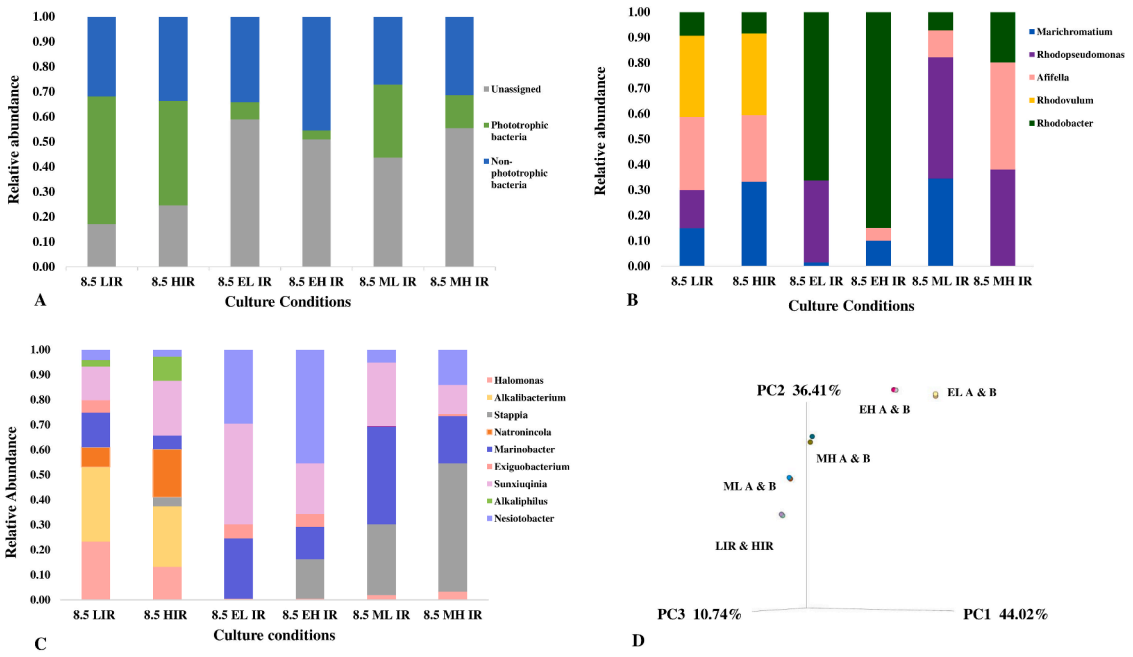

Fig. 2. . QIIME 2 results showing relative abundance of operational taxonomic units (OTUs) for: (A) Phototrophic bacteria vs non-phototrophic bacteria identified from the cultures at a genus level (B) Dominant phototrophic bacteria identified from the cultures at a genus level (C) Dominant heterotrophic bacteria identified from the cultures at a genus level (D) Representation of beta diversity obtained from QIIME 2 analysis of the four different cultures using the principal coordinate axis (PCoA), based on the Bray-Curtis dissimilatory method. ($n = 2$). LIR – pre-FACS cultures grown under low IR light; HIR- pre-FACS cultures grown under high IR light; EL- enriched low IR light; ML – mixed low IR light; EH – enriched high IR light and MH – mixed high IR light.

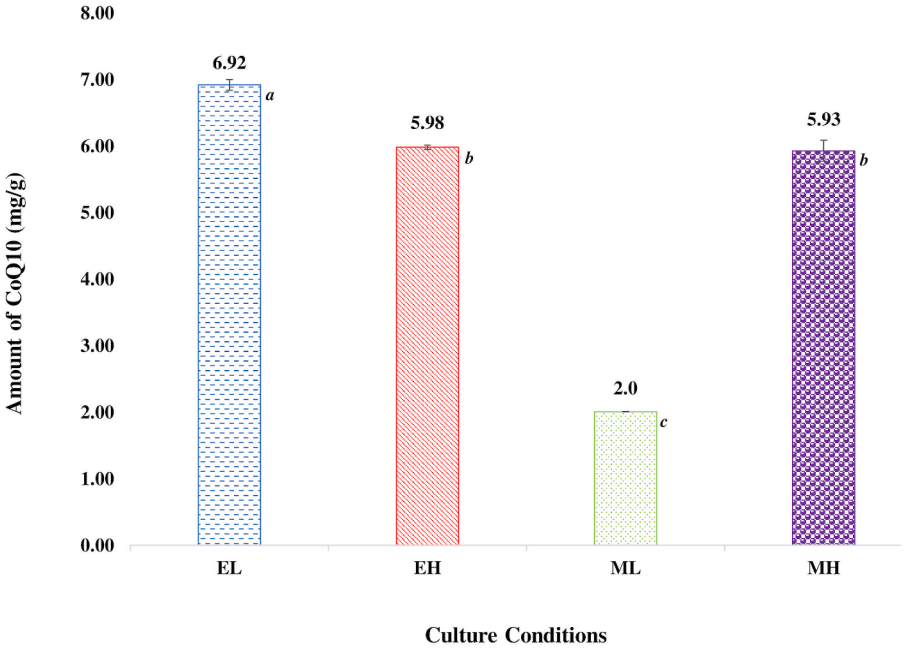

Fig. 3. The amount of CoQ_{10} recovered from enriched and mixed cultures under low and high IR light conditions, based on dry cell weight. EL- enriched low IR light; ML – mixed low IR light; EH – enriched high IR light and MH – mixed high IR light. $n = 2$. Significance was analyzed using Tukey's test where $p < 0.05$ was taken as the level of significant difference. Same letter superscripts denote no significant difference ($p > 0.05$); different letter superscripts denote a significant difference at $p < 0.05$.

enriched culture. Thus, when the post-FACS cultures were compared to the pre-FACS cultures, enriched cultures under low IR light conditions and high IR light conditions had the lowest proportion of operational taxonomic units (OTUs) associated with phototrophic bacteria, < 10%, compared to the non-phototrophic bacteria (refer Fig. 2**A**). On the other hand, the mixed low and high IR light conditions resulted in a higher proportion of OTUs associated with phototrophic bacteria, 30% and over 10%, respectively. Overall, the proportion of OTUs associated with phototrophic bacteria for the EL, EH, ML and MH cultures was much lower than that of the original seed sources, low IR light seed (LIR) and high IR light seed (HIR). The seed sources had over 40–50% of OTUs associated with phototrophic bacteria (refer Fig. 2**A**).

The QIIME 2 analysis revealed that there were no genera associated with oxygenic phototrophs identified in the cultures, instead all the phototrophic bacteria reported at the genus level were anoxygenic phototrophic bacteria, specifically purple non-sulfur bacteria of the following genera: *Rhodovulum, Afifella, Rhodobacter and Rhodopseudomonas;* and purple sulfur bacteria of the genus *Marichromatium.*

From the distribution of OTUs at a genus level for anoxygenic phototrophic bacteria, it was clear that compared to the LIR (low IR light)

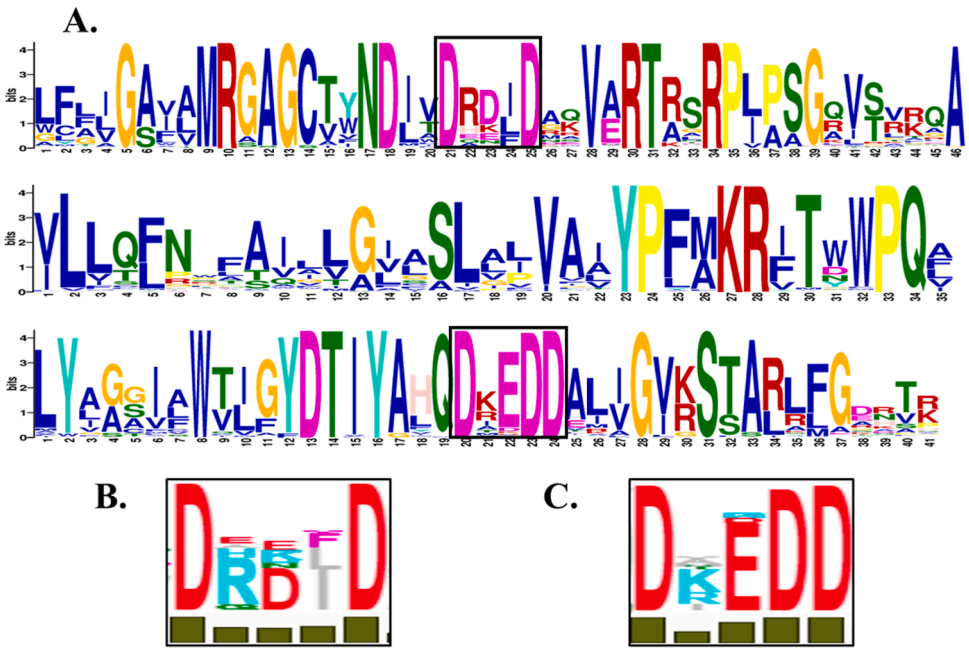

Fig. 4. Conserved Motifs. A) Sequence logo of most significant three motifs, designated by MAST tool (3) conserved among 4038 UbiA enzyme sequences sharing 40% identity. B) and C) Sequence logo of the Asp-rich segment within Motif I and Motif III with conservation weights derived by Multiple Sequence alignment of bacterial UbiA protein sequences.

and HIR (high IR light) seed sources, there were lower proportions of OTUs associated with *Afifella* for EH (~5%), ML (10%) and MH (~50%) cultures, and there were no OTUs associated with *Rhodovulum* for these cultures. For the EL cultures however, there were no OTUs representing either *Afifella* or *Rhodovulum* (refer Fig. 2**B**). A higher proportion of OTUs belonging to the *Rhodobacter* genus was observed in both the EL (~65%) and the EH (~85%) cultures compared to the mixed cultures and the seed source (refer Fig. 2**B**). On the other hand, a high proportion of OTUs related to *Rhodopseudomonas* was observed in ML (~50%) and MH (~35%) (see Fig. 2**B**), which could be due to its metabolic flexibility and ability to switch to various modes of nutrition, enabling this genus to thrive in mixed culture conditions under both light conditions [83]. OTUs belonging to the genus, *Marichromatium*, were not identified in MH cultures and were found at very low proportions (< 2%) in the EL cultures. At a species level, four purple-non sulfur bacteria were identified and included: *Afifella pfennigii, Rhodovulum adriaticum, Rhodobacter blasticus* and *Rhodovulum marinum*. The dominant genera of non-phototrophs or heterotrophic bacteria present in the EH, EL, MH and ML cultures are *Stappia, Marinobacter, Sunxiuqinia, Exiguobacterium* and *Nesiotobacter* (refer Fig. 2**C**).

The PCoA plot exhibits the differences between the bacterial communities present in our cultures. Since HIR and LIR are the seed samples (pre-FACS), as expected, they are clustered together due to the similarity in their community composition. ML cultures seems to have the most similar community composition to the seed samples, followed by MH cultures (refer Fig. 2**D**). EL and EH are quite similar in their community composition and are thus clustered together; however, they are farthest from the seed cultures (LIR and HIR) due to the differences in their community composition.

3.2. CoQ_{10} estimation

The highest amount of CoQ_{10} was reported for the enriched cultures under low IR light (EL cultures) at 6.92 mg/g dry cell weight (DCW), while the lowest amount was estimated from mixed cultures under low light conditions (ML cultures) at 2.0 mg/g DCW, and these were statistically different ($p < 0.05$) from the remaining cultures (refer Fig. 3.). However, there was no statistical difference between the EH and MH in the amount of CoQ_{10} recovered. The enriched cultures, EL and EH, produced higher amounts of CoQ_{10} compared to the mixed cultures. This could be because CoQ_{10} is lipophilic in nature [84] and may have been stained by the Nile red stain, and consequently selected during FACS to constitute the enriched cultures.

3.3. Discovery of conserved motifs by protein sequence cluster analysis

We queried using the search term "4-Hydroxybenzoate octaprenyl transferase" in the UniProt protein database [62] and it yielded 22,379 entries prevalent in various organisms. Further removal of entries annotated with the term 'probable' or 'putative' and those with protein sequences shorter than 200 base pairs, resulted in a protein sequence dataset of 17,980 sequences (refer **Table S1**). This dataset was first clustered into 28 clusters by sensitive protein sequence searching using MMseqs2 tool [63], where sequences in each cluster shared 30% identity with minimum coverage of 50%. Cluster 19 was the largest cluster consisting of 17,871 sequences (refer **Table S2.**). Sequences from Cluster 19 were input in MMseqs2 tool [63] to distill and identify sequence clusters sharing 40% identity with minimum coverage of 80%, resulting in 35 clusters. The largest cluster, Cluster-35 with 4038 sequences (refer **Table S3.**) incorporated all the sequences listed in Table 1., except for the sequence from *P. aeruginosa.*

Discovery of conserved un-gapped motifs shared by the 4038 protein sequences in Cluster 35 was done using the MAST tool [64] in MEME online suite [65]. Three most significant motifs:

Motif I - 'LFLIGAVAMRGAGCTYNDIVDRDIDAQVARTRSRPIPS GQVSVRQA', Motif II 'VLLQFNWFAILLGIASLALVAIYPFMKRITWW PQA' and Motif III 'LYAGGIAWTIGYDTIYAHQDKEDDALIGVKSTARLF GDRTR' with matches having a position p-value < 0.0001 were identified among these 4038 sequences, as shown in Fig. 4**A**. The discovered motifs encompass the Asp-rich segment postulated by several studies for prominent interaction with PHBA and GSPP [41,42] (refer **Fig. S4**).

Multiple sequence alignment of the bacterial UniProt entries (3921 sequences) among the 4038 sequences revealed the constituent residue patterns within the Asp-rich segments predominant in bacterial UbiA. The Asp-rich segments from Motif I comprised of the pattern D(E/A/H/R/Q)(E/K/H/N/D)(Y/F/L/I)D with highly conserved 1st & 5th residues

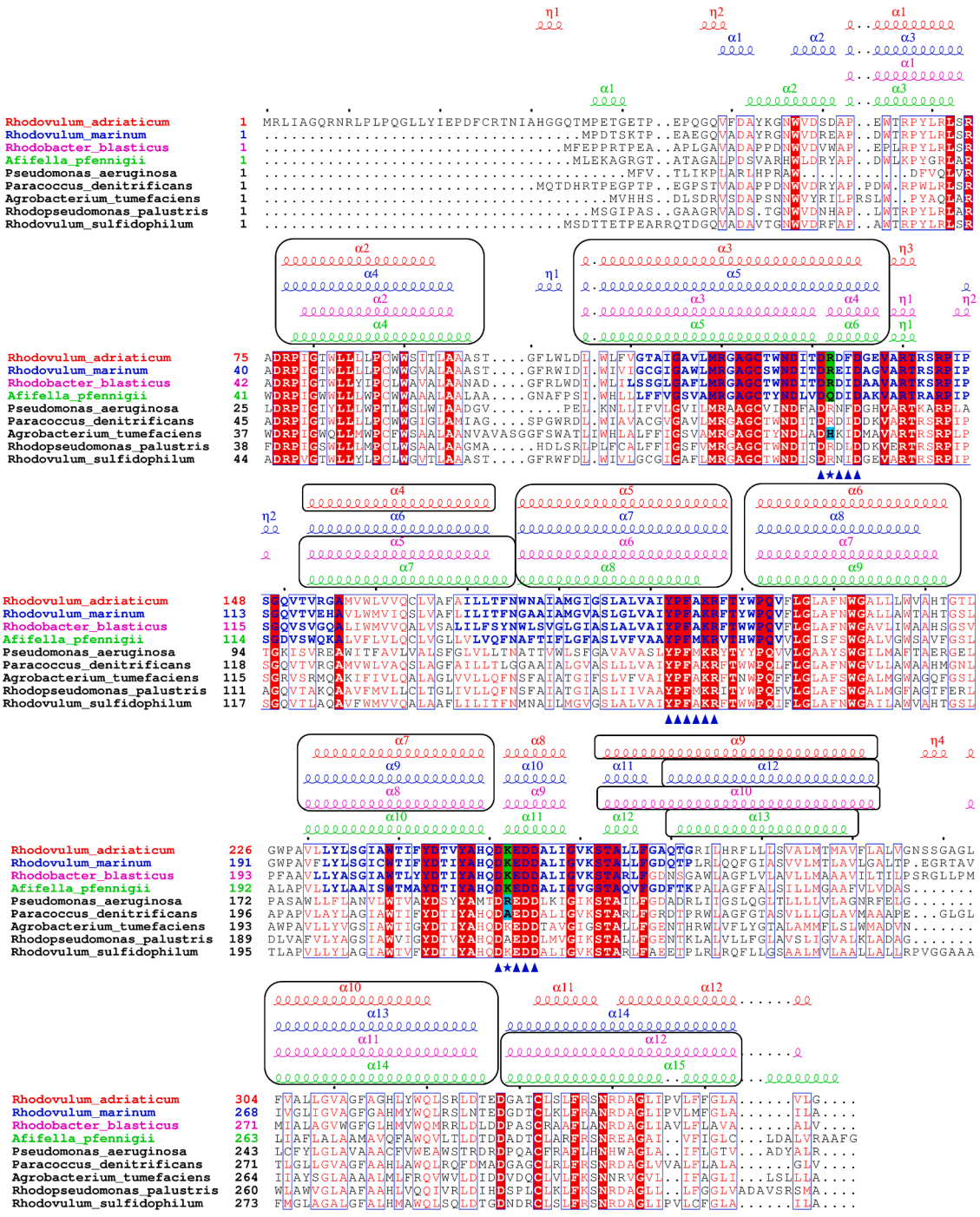

Fig. 5. Representation of Multiple sequence alignment of UbiA sequence from candidate organisms - *R. adriaticum, R. marinum, R. blasticus* and *A. pfennigii,* labeled in red, blue, pink and green, respectively, with industrial and native producers of CoQ_{10} - *P. aeruginosa, P. denitrificans, A. tumefaciens, R. palustris and R. sulfidophilum* using ESPript [85]. The secondary structures of candidate organisms predicted by I-TASSER are rendered in colors respective to the color of species label. And the transmembrane helices are marked by black boxes. Conserved motifs discovered by cluster analysis are highlighted in blue font with the Asp-rich motif marked by blue triangles. Residues designated for mutation and the corresponding template (H – *A. tumefaciens*, R - *P. aeruginosa* and A – *P. denitrificans*) are highlighted in green and marked by blue stars.

and moderately conserved 2nd, 3rd & 4th residues (refer **Fig. 4B**), Motif III comprised of the pattern D(V/A/M/T/K/R/I)(K/R/D/E)DD with highly conserved 1st, 4th & 5th residues, moderately conserved 3rd residue and a variable 2nd residue, as shown in **Fig. 4C**.

3.4. Selection of amino acid residues for mutation

To augment the substrate binding affinity of the UbiA enzyme to its ligands, this study proffers substitution of three residues in two potential mutation sites within the Asp-rich segment in the conserved motifs – Motif I and III for further in-silico screening studies. These two mutation sites were selected with the rationale that the inherent amino acid residues in these sites were well conserved among the four purple photosynthetic bacteria but different in the native/industrial bacterial species. The three residues, namely, histidine (H), arginine (R) and alanine (A) were selected for substitution at these mutation sites based on 3 native

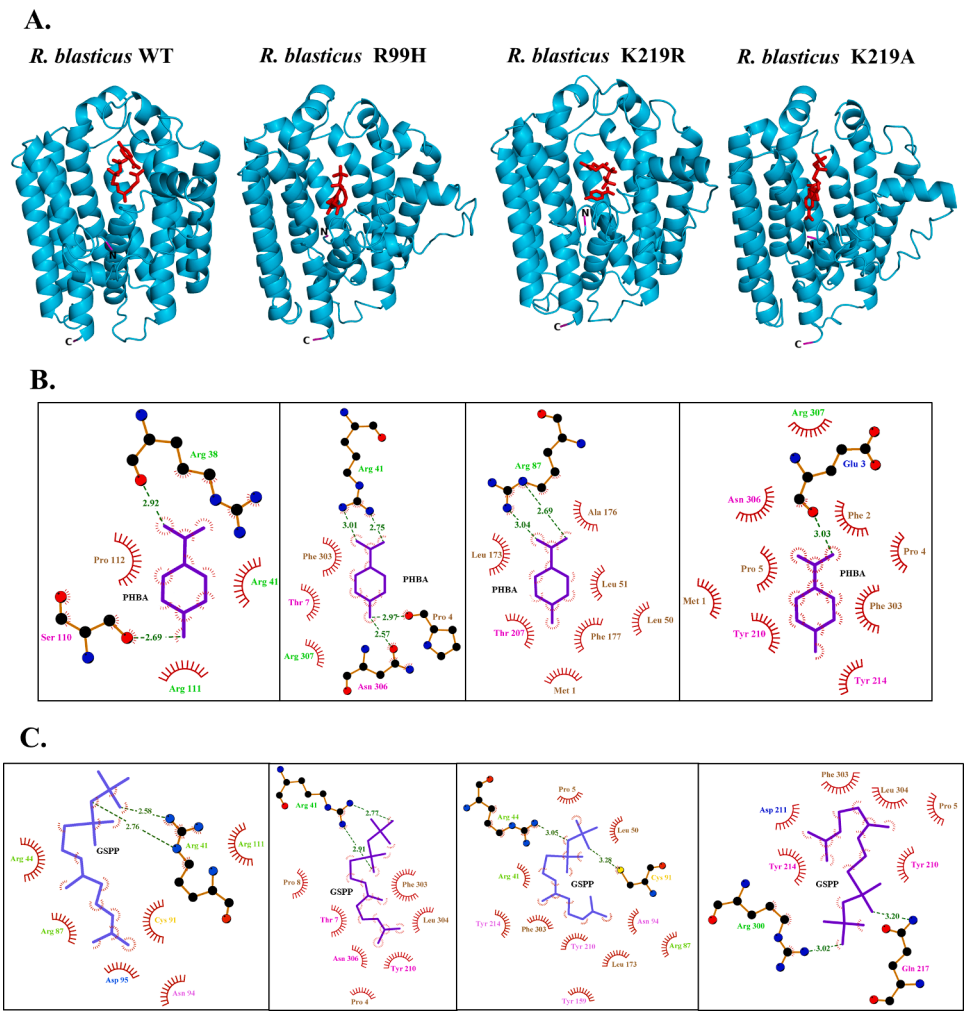

Fig. 6. Protein-ligand interactions of UbiA from *R. blasticus*: A) Cartoon representation of docked protein (represented in cyan) – ligand (represented in red) complexes of original UbiA and the subsequent mutant proteins from *R. blasticus*. B) The Ligplot interaction plot of amino acids from the respective protein kind with PHBA ligand and C) GSPP ligand. The polar uncharged, polar negatively charged, polar positively charged, non-polar and cysteine amino acid residues are highlighted in magenta, blue, green, brown, and yellow respectively.

CoQ_{10} producers. Residue H substitution was based on the UbiA protein sequence of *A. tumefaciens*. Firstly, the italicized residues inherent in the Asp-rich segment of Motif I for *R. blasticus* – DRDID, *R. adriaticum* – DRDFD, *A. pfennigii* – DQDID and *R. marinum* – DRDID, were replaced with H. This generated the following mutants: *R. blasticus* – R99H, *R. adriaticum* – R132H, *A. pfennigii* – Q98H and *R. marinum* – R97H. Next, the 2nd residue in the Asp-rich segment of Motif III (all species - DKEDD) was replaced with residues R and A, as shown in Fig. 5. Finally, the R and A substitutions were based on UbiA protein sequences of *P. aeruginosa* and *P. denitrificans*, respectively. This generated the following mutants: *R. blasticus* – K219R/A, *R. adriaticum* – K252R/A, *A. pfennigii* – K218R/A and *R. marinum* – K217R/A.

3.5. Generating I-TASSER models for docking studies

Despite the numerous research studies on UbiA enzymes, X-ray crystallographic structures of only two members, *A. pernix* UbiA, PDB: 4OD4 [86] and *Archaeoglobus fulgidus* UbiA, PDB: 4TQ5 [87], have been reported due to the complexities associated with experimental determination of protein structures. Nevertheless, prediction of three-dimensional structures of proteins using computational methods has proved to be a feasible alternative approach. I-TASSER is one of the state of the art template-based modeling tools for protein structure prediction which has repeatedly been the highest-rated tool by the scientific community as per the Critical Assessment of Structure Prediction (CASP) experiments [88], due to its reliability in terms of experimental accuracy [89]. Although deep learning based modeling tools like AlphaFold2 [90] have outperformed recent CASP experiments, significant number of predicted protein structures lacked experimental accuracy [88].

As a comparative study, the protein sequence of UbiA from *A. pernix* K1deposited in PDB, 4OD5 was retrieved and the three-dimensional protein structure was modelled using I-TASSER and the AlphaFold2 model for same protein was downloaded from UniProt. Bound ligands from 4OD5 structure were removed and superposed over both models. The apo 4OD5 structure superposed (C-α atoms) upon I-TASSER model and AlphaFold2 model with a total Root-Mean-Square-Deviation (RMSD) of 0.55 Å and 1.068 Å respectively. The I-TASSER derived model better aligned to the experimental structure when compared to the AlphaFold2 derived model (**Fig. S5 A&B**). Therefore, the three-dimensional structures of the wild-type and mutant UbiA enzymes listed in **Table 1.**, were predicted using the I-TASSER protein modeling server. For each input protein sequence, I-TASSER predicts five energy minimized structural models (Model 1–5) ordered based on their c- score (confidence score derived from significance of threading alignments and residue-level local quality) [66–68].

Model 1 from the I-TASSER results was selected for the subsequent analysis, except for the wild-type protein from *R. marinum*, where Model 3 was chosen for conducive protein folding. The c-score values for the modelled structures were quite significant and varied between -1.88 to 0.70. All the modelled structures were similar in their structural architecture, forming α-helical barrels with 7–9 antiparallel helices and a central cavity.

The quality of the three-dimensional protein models generated by I-

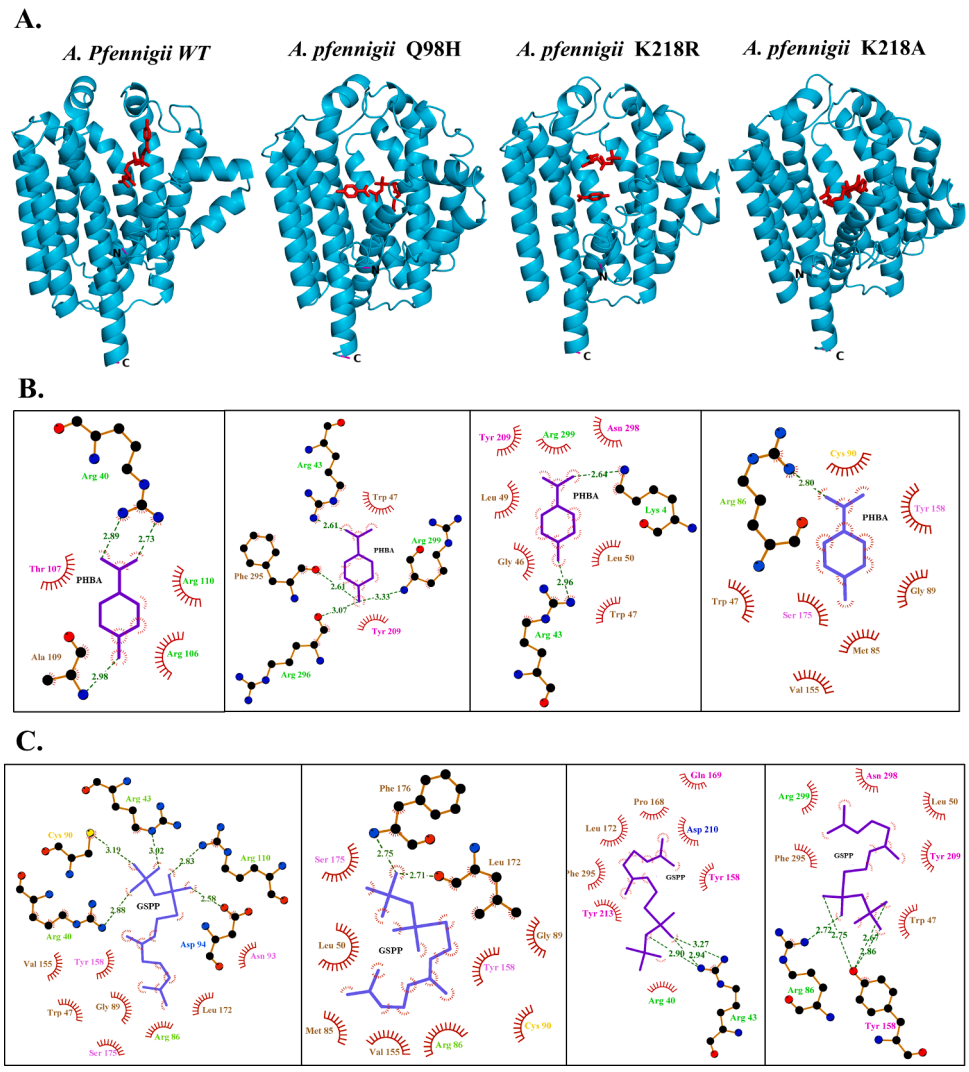

Fig. 7. Protein-ligand interactions of UbiA from *A. pfennigii*: A-C) Details are the same as described for Fig. 6.

TASSER was evaluated in terms of its stereochemistry using PROCHECK. For all the models, the Phi and Psi angles of more than 97% residues were present in the allowed region of Ramachandran plots (**Fig. S2**). Next, ProSA program was used to assess whether the predicted models were comparatively accurate and reliable as experimentally determined protein structures (**Fig. S3**). The Z-score plot output of ProSA program is comparative representation of the Z-score (a cumulative measure of model quality and energy distribution) of the input structural model against the Z-scores of all similarly sized experimentally determined proteins (both X-ray and NMR structures) in PDB. Z- scores of all the predicted models were within the range of experimental protein structures (**Fig. S3**).

Protein sequences of UbiA enzyme from the four purple photosynthetic bacteria used in this study differed in the length, *R. blasticus* – 323 residues, *R. adriaticum* – 356 residues, *A. pfennigii* – 320 residues and *R. marinum* – 320 residues. The transmembrane topology of the UbiA enzymes from the four PNSBs varied across the species. Typically, each of the enzymes were comprised of 7–9 transmembrane α-helices (*R. adriaticum* and *A. pfennigii* - 8 transmembrane α-helices, *R. marinum* - 7 transmembrane α-helices and *R. blasticus* - 9 transmembrane α-helices) as depicted in Fig. 5. The Asp-rich motifs – Motif I and Motif III (with selected mutation sites) of the UbiA enzymes from *R. adriaticum* and *R. blasticus* (shared identity-62%, **Table S4**) were inherent in the cytoplasmic loops similar to the UbiA enzyme of *Archaeoglobus fulgidus* [87]. However, in the UbiA enzymes from *R. marinum* and *A. pfennigii* (shared identity-49%, **Table S4**), Motif I was integral to a cytoplasmic loop while Motif III was integral to an extracellular loop (**Fig. S6**). This suggests that though the substrate-binding sites of enzymes from UbiA family were well conserved, the structural topology varied across different species.

3.6. UbiA enzyme MLSD studies

Three-dimensional structures of ligands – PHBA and GSPP were obtained from the substrate-bound structure of UbiA enzyme of *A. pernix* K1 (PDB ID: 4OD5) from the RSCB protein data bank (PDB) [86], and utilized for MLSD with I-TASSER generated protein models of the wild-type and mutant UbiA enzymes listed in Table 1. MLSD was performed using the MTiAutodock 4.2.6 webserver and the protein-ligand docking score in kcal/mol was thus determined. The MLSD results are summarized in **Table S5**.

The MLSD of wild-type and mutated UbiA proteins from *R. blasticus* with PHBA and GSPP ligands revealed that the protein-ligand complex from K219A mutant exhibited the best docking score, -3.60 kcal/mol, even better than the protein-ligand complex from the template organism, *P. denitrificans,* based on which the mutation was designated (refer **Table S5.**). Hydrogen bonds were formed between PHBA and E3 (polar-negatively-charged/acidic residue); GSPP and Q217 (polar-uncharged residue) and R300 (polar-positively-charged/basic residue) as seen in Fig. 6.

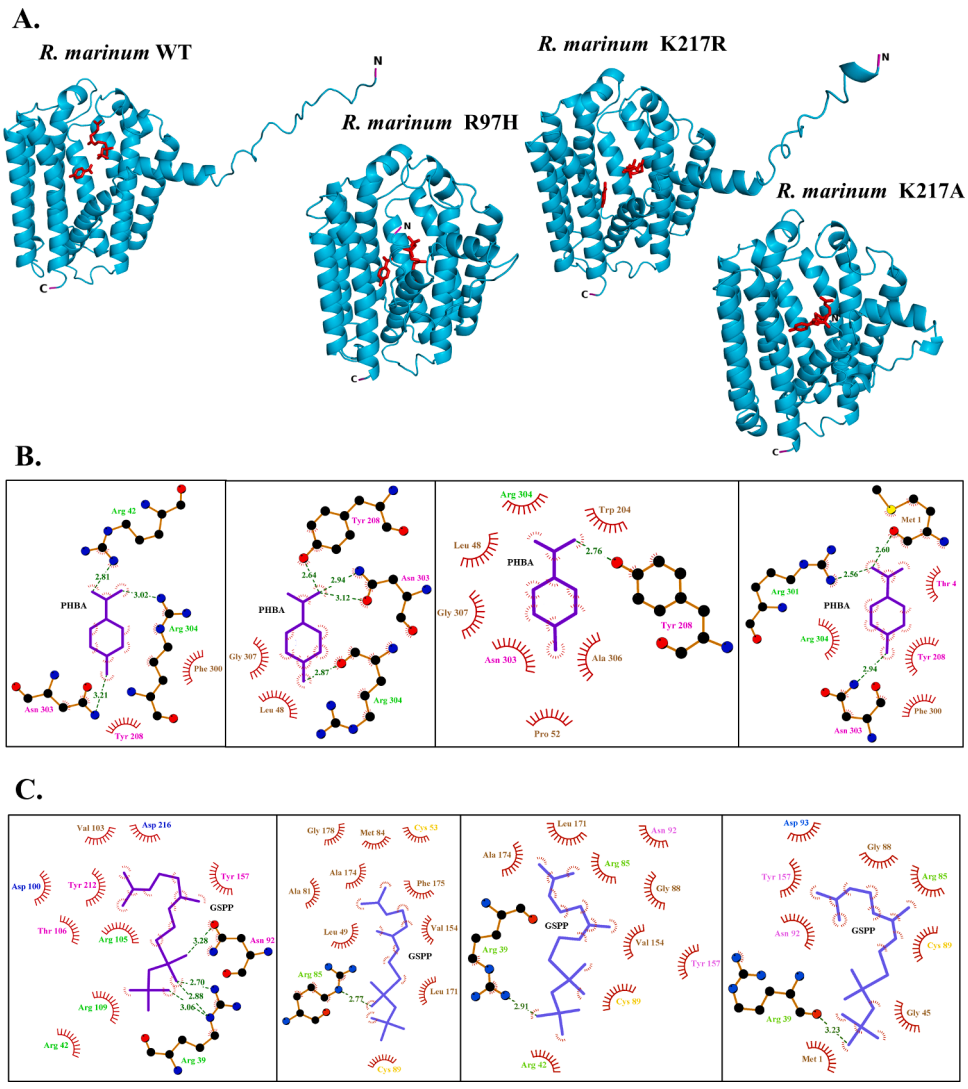

Fig. 8. Protein-ligand interactions of UbiA from *R. marinum*: A-C) Details are the same as described for Fig. 6.

In the case of wild-type and mutated UbiA proteins from *A. pfennigii*, K218R mutant had the best docking score of -4.32 kcal/mol, which was over 1.5 times greater than the protein-ligand complex from the template organism, *P. aeruginosa*, that exhibited a docking score of only -2.46 kcal/mol (refer **Table S5.**). Hydrogen bonds were formed between PHBA and K4 (polar-positively-charged/basic residue) and both PHBA & GSPP, with R43 (polar-positively-charged/basic residue) as seen in Fig. 7.

Among the wild-type and mutated UbiA proteins from *R. marinum*, best docking score, -4.45 kcal/mol, was displayed for the protein-ligand complex from R97H mutant. This value was greater than that of the template organism, *A. tumefaciens* (-2.85 kcal/mol), as seen in **Table S5**. Hydrogen bonds were formed between PHBA with Y208 (polar-uncharged residue), N303 (polar-uncharged residue) and R304 (polar-positively-charged/basic residue); GSPP and R85 (polar-positively-charged/basic residue) as seen in Fig. 8. In addition, we observed that among the residues forming hydrogen bonds, the Y208 residue, a potential phosphorylation site, formed a hydrogen bond with the PHBA substrate (refer **Table S5**).

As represented in Fig. 9. and **Table S5.**, the K252R mutant of *R. adriaticum* had the best docking score, -4.21 kcal/mol, compared to the other variants and wild-type UbiA proteins from the same organism. It even had a better docking score compared to the protein-ligand complex from the template organism, *P. aeruginosa*. As displayed in Fig. 9., hydrogen bonds were formed between PHBA and Q48 (polar-uncharged residue), F50 (non-polar), R340 (polar-positively-charged/basic residue) and L344 (non-polar); GSPP and A306 (non-polar).

Among the three template organisms utilized in this study the substrate bound UbiA enzyme belonging to *P. dentrificans* had the best docking score, -3.13 kcal/mol, while *P. aeruginosa* had the poorest docking score, -2.46 kcal/mol, as shown in Fig. 10 and **Table. S5**.

Huang et al. [87] have observed that substrate binding induces conformational changes in the enzymes of UbiA superfamily, especially in the loops that contain Motif I and Motif III. The crucial step in synthesis of CoQ_{10} by UbiA enzymes, is the prenylation of PHBA in its ortho position [91]. Upon substrate binding, these loops that surround the active site, transition from disordered state to ordered state to retain the substrate within the catalytic cavity of the enzyme. Probably, these flexible catalytically significant loops stabilize the enzyme into a closed conformation, upon binding of PHBA (prenyl acceptor) in the catalytic cavity. Since polyprenyl diphosphates like GSPP are negatively charged molecules, they enter the catalytic cavity of the enzyme majorly through the lateral portal that opens into the lipid bilayer. To assess the effect of presently studied mutations in protein flexibility, the dynamics of UbiA enzymes from the four PNSBs was analyzed using DynaMut2 tool [92]. Results from DynaMut2 include calculated differences in vibrational entropy and free energy between the wild-type and mutant structures. Probably, pertaining to the variation in structural topology, it can be

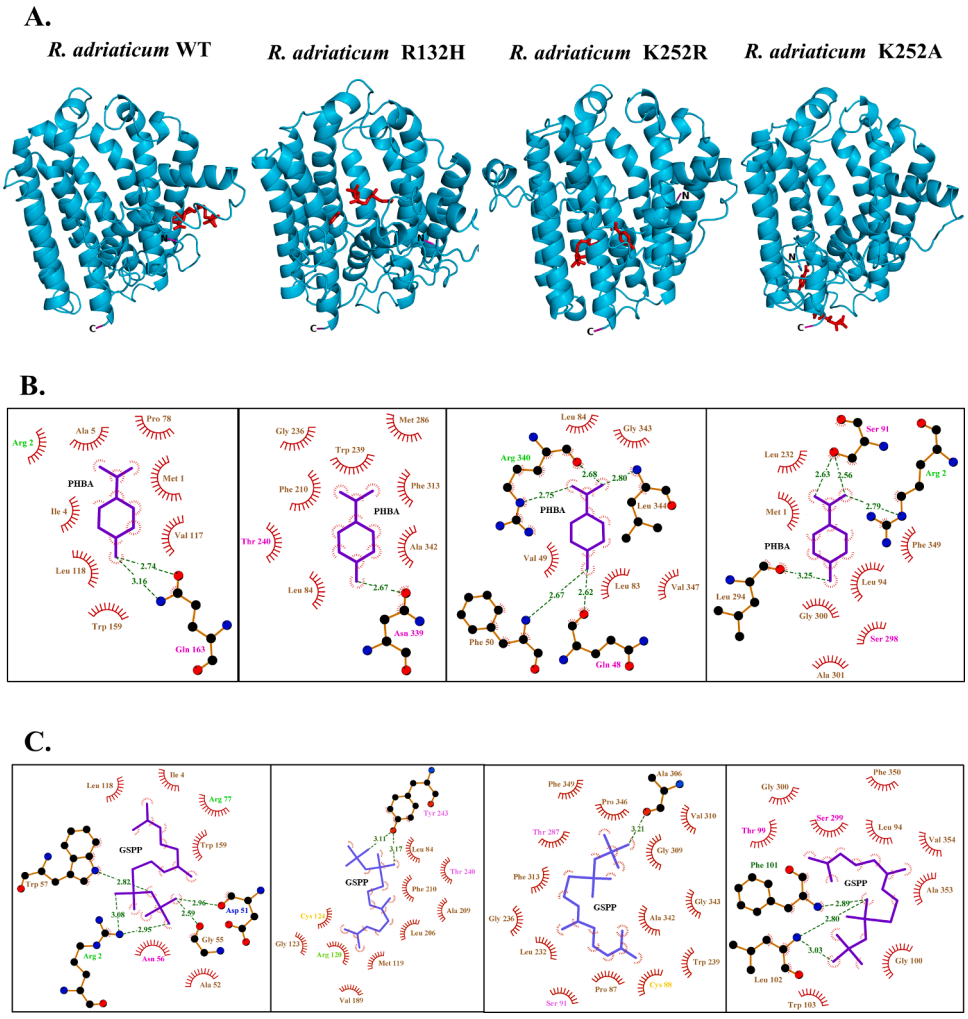

Fig. 9. . Protein-ligand interactions of UbiA from *R. adriaticum*: A-C) Details are the same as described for Fig. 6.

observed that the effect of mutations in the enzyme's flexibility, varied across species (**Fig. S7**).

Loss or gain of flexibility in each of the mutant protein, in terms of vibrational entropy was simultaneously analyzed with their docking scores derived from MLSD (**Fig. S7 and Table S6**). The following was observed from the best scoring mutants, which could have led to improved docking scores: (i) *R. adriaticum* K252R had a slight loss of vibrational entropy in Motif III, (ii) *R. marinum* R97H showed a slight loss of vibrational entropy in Motif I, (iii) *A. pfeniigii* K218R showed a slight gain of vibrational entropy in Motif III and (iv) *R. blasticus* K219A had a gain of vibrational entropy in Motif III. Further, when analyzed in terms of loss (destabilizing) or gain (stabilizing) of free energy in comparison to wild type enzyme, it was observed that (i) *R. adriaticum* K252R had gained, (ii) *R. marinum* R97H had lost, (iii) *A. pfeniigii* K218R had slightly lost and (iv) *R. blasticus* K219A had slightly gained free energy. This emphasizes the requirement for unique protein engineering strategies to improve the substrate reactivity of each enzyme.

4. Discussion

In this study, we identified four PNSBs, *R. adriaticum, R. marinum, A. pfennigii* and *R. blasticus,* from the microbial mat cultures of a mangrove ecosystem in Qatar. Given the excellent ability of PNSBs to survive in their harsh native environment, feasible growth conditions for large-scale culturing and indigeneity, they could be utilized as excellent microbial factories for production of $CoQ_{10,}$ a high-demand, high-value product. From the results of the study, we found that the amount of CoQ_{10} recovered from the EL cultures was the highest – 6.92 mg/g DCW, while the ML cultures had the least amount of CoQ_{10} at 2.0 mg/g DCW. Both the enriched cultures, EL and EH, were found to have higher CoQ_{10} compared to the mixed cultures, which could be a consequence of Nile red stain selection (during FACS) of these lipophilic CoQ_{10} molecules.

Although heterotrophic bacteria can also synthesize CoQ_{10}, among the dominant heterotrophs identified in this study (refer Fig. 2**C**) only bacteria belonging to the genus *Stappia* are known to synthesize CoQ_{10} [93]. The other heterotrophic bacteria identified in this study synthesized either CoQ_9 [94] or menaquinone [95,96]. Further, we observed a lower proportion of OTUs associated with the *Rhodobacter* genus (refer Fig. 2**B**), particularly *R. blasticus* in the ML cultures, which incidentally also had the least amount of CoQ_{10}. Several studies have utilized *Rhodobacter sphaeroides* to produce CoQ_{10} [33,56,97-99]. Yajima et al. [29] even have a patented method for producing CoQ_{10} from a mixed culture of bacteria, which included the PNSB *Rhodopseudomonas palustris* JCM 2524 90 6 and *Rhodobacter capsulatus* SB 1003 95 6. Similarly, there may be other species within the *Rhodobacter* genus, such as *R. blasticus* and other PNSB that were identified in this study that could synthesize CoQ_{10}.

The conserved catalytically significant Asp-rich motifs inherent in the protein sequences of the UbiA enzymes present in the identified PNSB were mapped to that of CoQ_{10} producing industrial strains to designate relevant mutations, and the improvement in substrate reactivity was computationally predicted by MLSD.

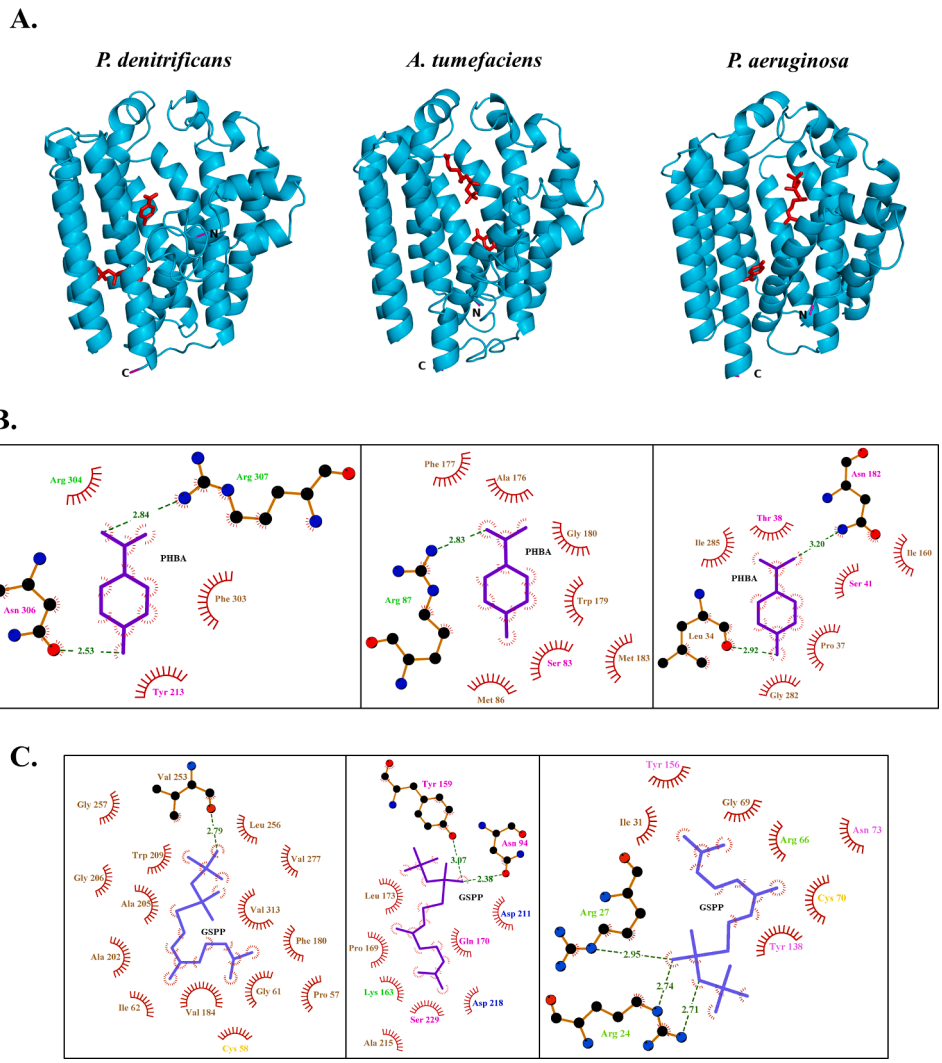

Fig. 10. . Protein-ligand interactions of UbiA from industrial/native CoQ_{10} producers: A) Cartoon representation of docked protein (represented in cyan) – ligand (represented in red) complexes of UbiA proteins from *P. denitrificans, A. tumefaciens* and *P. aeruginosa*. as described for Fig. 6.**B**, C) Details are the same as described for Fig. 6.

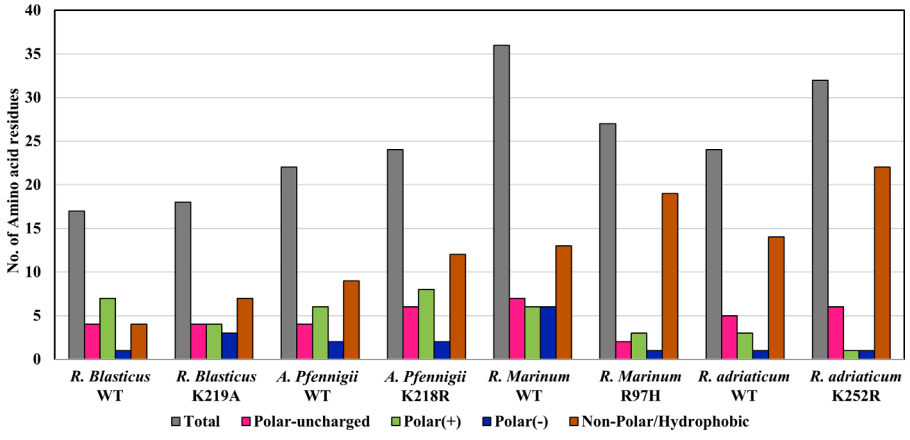

Fig. 11. . Physiochemical properties of the residue environment. Comparative boxplot representation of relative number of amino acids inherent in the interacting residue environment of wild-type (WT) and substantiated mutant protein-ligand complexes with improved substrate reactivity. The amino acid residues are categorized based on different physiochemical properties.

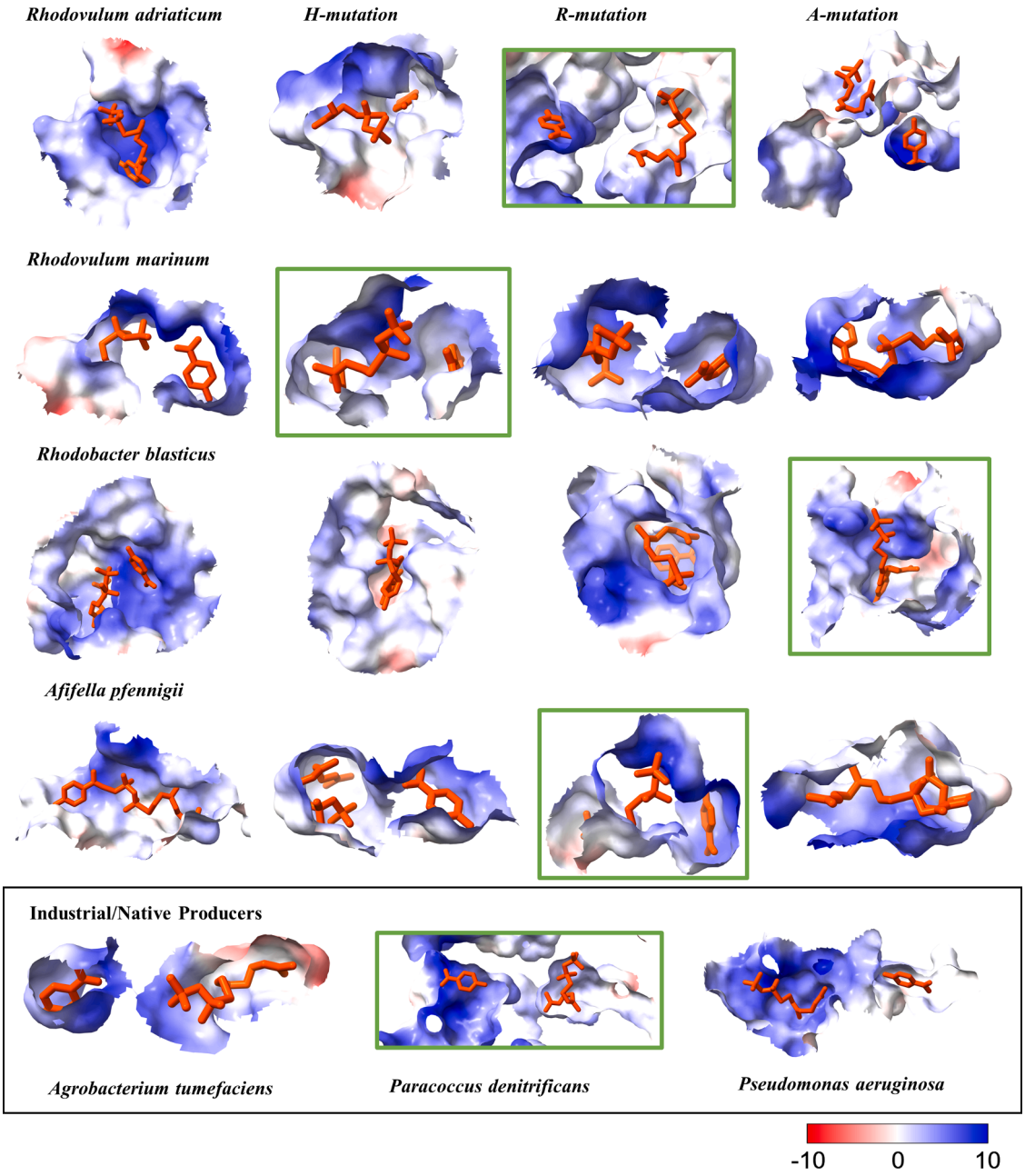

Fig. 12. . Electrostatic potential of binding pockets of protein-ligand docked complexes: Representation of electrostatic potential ranging from red for negative potential, white for zero and blue for positive potential of the ligand binding pockets of original and mutant UbiA proteins from candidate organisms and industrial/ native producers of CoQ_{10}. The protein-ligand complex with best docking score is highlighted in green box.

The MLSD results could aid in identifying the propitious residue environment conducive for enhanced substrate reactivity in UbiA, the key enzyme involved in biosynthesis of COQ_{10}. Enzymes facilitate chemical reactions by ushering one or more chemical reactants/ substrates side by side in an optimal orientation. It is the active site of an enzyme that binds to the substrate and is typically composed of a distinctive combination of amino acid residues. Amino acid residues are grouped into separate categories based on their physiochemical properties. The properties, structures, sequences, and positions of the amino acid residues constituting the active site of an enzyme, form a characteristic chemical environment that is designed for its substrate.

As a proof of concept, the substrate bound UbiA structure PDB:4OD5 was compared with the MLSD derived predicted protein-ligand complex (refer **Fig. S5**). Both protein-ligand complexes were similar in terms of the interacting residue environments for ligands PHBA and GSPP, with most constituent residues in common, though the ligand orientations were different. This revealed the adequacy of prediction of protein-ligand complexes using MLSD. The protein-ligand complexes of wild-type and mutant UbiA enzymes of the four purple photosynthetic bacteria derived from MLSD were studied extensively to identify the characteristic chemical environment that ameliorated substrate binding affinity of the propitious mutant enzymes. We hypothesize that the improved binding affinity observed in the propitious mutant enzymes can be attributed to an amalgamation of several factors such as: (i) hydrogen bonds formed between the enzyme and substrate (ii) physiochemical properties of the residue environment in enzyme-substrate interaction site (iii) electrostatic potential of the enzyme-substrate interaction site and (iv) proximity of enzyme-substrate interaction site residues to potential phosphorylation sites and (v) gain or loss of flexibility in loops surrounding the catalytic cavity.

Localization of non-polar and polar amino acid residues are characteristic of an enzyme's kind and function. UbiA is a membrane protein, and these proteins are inclined to contain non-polar amino acids on their surfaces that interact with the cell membrane and polar amino acids in their internal pores to form hydrophilic channels. Among the studied protein-ligand complexes, the majority of the amino acid residues involved in hydrogen bond formation with the ligands were polar-positively-charged/basic residues, and polar-uncharged in nature. This is in line with findings reported by Li [100] and Ren et al. [42], suggesting the involvement of the conserved motifs of UbiA in the recognition of the ligands via polar amino acid residues lining its internal channels. Internal substrate access channels of the enzyme are critical for its catalytic activity, and the introduction of mutations in these tunnels can affect its substrate specificity [101]. From **Fig. 11.**, it could be speculated that the substantiated mutant UbiA proteins has improved substrate reactivity, attributed to the balanced, rather than skewed, distribution of non-polar and polar amino acid residues lining their internal substrate access channel.

The catalytic potential of an enzyme is majorly influenced by the electrostatic environment of its active site [102]. Computational analysis of the interaction sites of the derived protein-ligand complexes could aid in estimation of preorganization of the electrostatic environment surrounding the active site of an enzyme. Investigation of the electrostatic potential of the protein-ligand interaction environment indicated that the electrostatic potential of interaction sites of propitious mutant UbiA proteins ranged from neutral to slightly positive when compared to the wild-type and unpropitious mutants (refer **Fig. 12**). In the case of *R. adriaticum* and *R. marinum*, the respective K252R and R97H propitious mutants exhibited an electrostatic environment of protein-ligand interaction sites that tended to range between slightly blue to white. While in *R. blasticus,* though the electrostatic environment of protein-ligand interaction site of R99H mutant looks the palest, the K219A mutant exhibited better binding affinity probably due to the appearance of pink hue (negatively charged residues) in the former. In *A. pfennigii,* the wild-type and all the mutant proteins had similarly colored (slight blue to white) electrostatic environments of their protein-ligand interaction sites correlating with similar binding affinity of all the protein-ligand complexes. Furthermore, we could observe overrepresentation of the residue Y, over S and T among the predicted phosphorylation sites, across all four purple photosynthetic bacteria (refer **Table S5**). And many of the phosphorylation sites were prevalent among the interacting residue environment of the protein-ligand complexes.

Though this study is a computational approach to substantiate potential mutants of four PNSB UbiA enzymes with augmented substrate binding affinity, follow-up experimental investigation is required to corroborate these results.

5. Conclusion

From the microbial mat cultures, we were able to enrich and identify, through 16S rRNA sequencing, four purple photosynthetic bacteria with potential to biosynthesize CoQ_{10}. We employed comparative sequence analysis of all available UbiA protein sequence dataset, including industrial/native producers of COQ_{10} and MLSD to screen for potential point mutations, present in these four purple photosynthetic bacteria, at motifs conserved across the entire protein dataset of UbiA enzymes. All the substantiated mutant proteins had improved binding affinity values compared to their respective wild-type protein, even better than the template organisms based on which the mutations were designated. In addition, the in-depth investigation of the identified interacting residues prevalent in the enzyme-substrate complexes of the wild-type and mutated proteins, revealed the influence of their inherent structural architecture, physiochemical properties, and electrostatic potential in the substrate binding affinity of the enzyme. Therefore, we propose that an elevation in the catalytic efficiency of the UbiA enzyme can be achieved by protein engineering the substrate residue environment to improve the substrate binding affinity of the enzyme with its substrates. The findings from this study will lay the necessary premise for future laboratory-based experimentation.

Supplementary material

Supplementary Table S1.xlsx – Dataset of Protein Sequence entries of 4-Hydroxybenzoate octaprenyl transferase derived from UniProt database. This dataset was input to MMseqs2 tool for sensitive sequence search for Clustering analysis.

Supplementary Table S2.xlsx – Dataset of Largest Cluster, Cluster-19 identified during first step of clustering using MMseqs2 tool. Protein Sequences share 30% sequence identity and 50% minimum coverage.

Supplementary Table S3.xlsx – Dataset of Largest Cluster, Cluster-35 identified during Second step of clustering using MMseqs2 tool. Protein Sequences share 40% sequence identity and 80% minimum coverage.

Declaration of Competing Interest

The authors declare that they have no known competing financial interests or personal relationships that could have appeared to influence the work reported in this paper.

Data availability

Data will be made available on request.

Acknowledgements

The graphical abstract was created using BioRender.com. The authors appreciate the financial and technical support of Qatar National Research Fund (grant NPRP11-S-0110–180245). Open Access funding provided by Qatar National Library

Supplementary materials

Supplementary material associated with this article can be found, in the online version, at doi:10.1016/j.btre.2022.e00775.

References

[1] R. Lordan, Dietary supplements and nutraceuticals market growth during the coronavirus pandemic - implications for consumers and regulatory oversight, PharmaNutrition 18 (2021), 100282, https://doi.org/10.1016/j.phanu.2021.100282.
[2] G.M. Insights, Coenzyme Q10 Market Size By Application (Pharmaceuticals, Dietary Supplements, Cosmetics) Industry Analysis Report, Regional Outlook, Application Potential, Covid-19 Impact Analysis, Competitive Market, Price Trend, 2021, pp. 2021–2027.
[3] Fact.M.R. (2021) Coenzyme Q10 Market. https://www.factmr.com/report/732/coenzymes-q10-market [accessed on 17 July 2022].
[4] K. Zmitek, et al., The effect of dietary intake of coenzyme Q10 on skin parameters and condition: results of a randomised, placebo-controlled, double-blind study, Biofactors 43 (2017) 132–140, https://doi.org/10.1002/biof.1316.
[5] K. Zmitek, et al., Effects of a combination of water-soluble coenzymeQ10 and collagen on skin parameters and condition:results of a randomised, placebo-controlled,double-blind study, Nutrients (2020) 12, https://doi.org/10.3390/nu12030618.
[6] K. Mizuno, et al., Antifatigue effects of coenzyme Q10 during physical fatigue, Nutrition 24 (2008) 293–299, https://doi.org/10.1016/j.nut.2007.12.007.
[7] V.Z. Lankin, et al., Mechanisms of oxidative modification of low density lipoproteins under conditions of oxidative and carbonyl stress, Biochemistry (Moscow) 72 (2007) 1081–1090, https://doi.org/10.1134/S0006297907100069.
[8] E. Lagoutte, et al., Oxidation of hydrogen sulfide remains a priority in mammalian cells and causes reverse electron transfer in colonocytes, Biochim. Biophys. Acta 1797 (2010) 1500–1511, https://doi.org/10.1016/j.bbabio.2010.04.004.
[9] I. Bogeski, et al., Calcium Binding and Transport by Coenzyme Q, J. Am. Chem. Soc. 133 (2011) 9293–9303, https://doi.org/10.1021/ja110190t.
[10] C.M. Quinzii, et al., CoQ10 deficiency diseases in adults, Mitochondrion 7 (Suppl) (2007) S122–S126, https://doi.org/10.1016/j.mito.2007.03.004.

[11] V.I. Zozina, et al., Coenzyme Q10 in cardiovascular and metabolic diseases: current state of the problem, Curr. Cardiol. Rev. 14 (2018) 164–174, https://doi.org/10.2174/1573403X14666180416115428.

[12] M. Alcázar-Fabra, et al., Clinical syndromes associated with coenzyme Q10 deficiency, Essays Biochem. 62 (2018) 377–398, https://doi.org/10.1042/ebc20170107.

[13] L.V. Schottlaender, et al., Coenzyme Q10 Levels are decreased in the cerebellum of multiple-system atrophy patients, PLoS ONE 11 (2016), e0149557, https://doi.org/10.1371/journal.pone.0149557.

[14] M. Arenas-Jal, et al., Coenzyme Q10 supplementation: efficacy, safety, and formulation challenges, Comprehensive Rev. Food Sci. Food Safety 19 (2020) 574–594, https://doi.org/10.1111/1541-4337.12539.

[15] S. Shukla, K.K. Dubey, CoQ10 a super-vitamin: review on application and biosynthesis, 3 Biotech. 8 (2018) 249, https://doi.org/10.1007/s13205-018-1271-6.

[16] H. Yoshida, et al., Production of ubiquinone-10 using bacteria, J. Gen. Appl. Microbio.l 44 (1998) 19–26, https://doi.org/10.2323/jgam.44.19.

[17] T. Urakami, M. Hori-Okubo, Production of isoprenoid compounds in the facultative methylotroph *Protomonas extorquens*, J. Fermentation Technol. 66 (1988) 323–332, https://doi.org/10.1016/0385-6380(88)90111-2.

[18] J.F. Imhoff, Quinones of phototrophic purple bacteria, FEMS Microbiol. Lett. 25 (1984) 85–89, https://doi.org/10.1111/j.1574-6968.1984.tb01381.x.

[19] A. Talaiekhozani, S. Rezania, Application of photosynthetic bacteria for removal of heavy metals, macro-pollutants and dye from wastewater: a review, J. Water Process Eng. 19 (2017) 312–321, https://doi.org/10.1016/j.jwpe.2017.09.004.

[20] A. Idi, et al., Photosynthetic bacteria: an eco-friendly and cheap tool for bioremediation, Rev. Environ. Sci. Bio/Technol. 14 (2015) 271–285, https://doi.org/10.1007/s11157-014-9355-1.

[21] K. Cao, et al., Photosynthetic bacteria wastewater treatment with the production of value-added products: a review, Bioresour. Technol. (2019), 122648, https://doi.org/10.1016/j.biortech.2019.122648.

[22] D.M. George, et al., An overview of anoxygenic phototrophic bacteria and their applications in environmental biotechnology for sustainable Resource recovery, Biotechnol. Rep. (Amst) 28 (2020) e00563, https://doi.org/10.1016/j.btre.2020.e00563.

[23] M.F. Tiang, et al., Recent advanced biotechnological strategies to enhance photo-fermentative biohydrogen production by purple non-sulphur bacteria: an overview, Int. J. Hydrogen Energy 45 (2020) 13211–13230, https://doi.org/10.1016/j.ijhydene.2020.03.033.

[24] M. Higuchi-Takeuchi, et al., Synthesis of high-molecular-weight polyhydroxyalkanoates by marine photosynthetic purple bacteria, PLoS ONE 11 (2016), e0160981, https://doi.org/10.1371/journal.pone.0160981.

[25] O.Z. Wada, et al., Single-cell protein production from purple non-sulphur bacteria-based wastewater treatment, Rev. Environ. Sci. Bio/Technol. (2022), https://doi.org/10.1007/s11157-022-09635-y.

[26] M. Sakarika, et al., Purple non-sulphur bacteria and plant production: benefits for fertilization, stress resistance and the environment, Microb. Biotechnol. (2019), https://doi.org/10.1111/1751-7915.13474.

[27] T. Kar Soon, et al., Isolation and characterization of purple non-sulfur bacteria, *Afifella marina*, producing large amount of carotenoids from mangrove microhabitats, J. Microbiol. Biotechnol. 24 (2014) 1034–1043, https://doi.org/10.4014/jmb.1308.08072.

[28] F. Meng, et al., One-step treatment and resource recovery of high-concentration non-toxic organic wastewater by photosynthetic bacteria, Bioresour. Technol. 251 (2018) 121–127, https://doi.org/10.1016/j.biortech.2017.12.002.

[29] Yajima, K. et al. (2018). Process for producing coenzyme Q10. Google patents.

[30] Alibaba. Coenzyme Q10. https://www.alibaba.com/showroom/coenzyme-q10.html [accessed on 17 July 2022].

[31] H. Thatoi, et al., Biodiversity and biotechnological potential of microorganisms from mangrove ecosystems: a review, Ann. Microbiol. 63 (2012) 1–19, https://doi.org/10.1007/s13213-012-0442-7.

[32] D. Roush, et al., A new niche for anoxygenic phototrophs as endoliths, Appl. Environ. Microbiol. 84 (2018), https://doi.org/10.1128/AEM.02055-17.

[33] L. Zhang, et al., Phosphate limitation increases coenzyme Q10 production in industrial *Rhodobacter sphaeroides* HY01, Synth. Syst. Biotechnol. 4 (2019) 212–219, https://doi.org/10.1016/j.synbio.2019.11.001.

[34] P. Li, et al., Relationship between coenzyme Q10 synthesis and cytochrome *accumulation* in *Rhodobacter sphaeroides* 2.4.1, in: H. Liu, et al. (Eds.), Advances in Applied Biotechnology, Springer, Singapore, 2018.

[35] C.P. Cluis, et al., The production of coenzyme Q10 in microorganisms, in: X. Wang, et al. (Eds.), Reprogramming Microbial Metabolic Pathways, Springer, Netherlands, 2012, pp. 303–326.

[36] M. Kawamukai, Biosynthesis of coenzyme Q in eukaryotes, Biosci. Biotechnol. Biochem. 80 (2016) 23–33, https://doi.org/10.1080/09168451.2015.1065172.

[37] K. Okada, et al., Cloning of the *sdsA* gene encoding solanesyl diphosphate synthase from *Rhodobacter capsulatus* and its functional expression in *Escherichia coli* and *Saccharomyces cerevisiae*, J. Bacteriol. 179 (1997) 5992–5998, https://doi.org/10.1128/jb.179.19.5992-5998.1997.

[38] K. Suzuki, et al., Evidence that Escherichia coli *ubiA* product is a functional homolog of yeast COQ2, and the regulation of *ubiA* gene expression, Biosci. Biotechnol. Biochem. 58 (1994) 1814–1819, https://doi.org/10.1271/bbb.58.1814.

[39] L. Aussel, et al., Biosynthesis and physiology of coenzyme Q in bacteria, Biochim. Biophys. Acta 1837 (2014) 1004–1011, https://doi.org/10.1016/j.bbabio.2014.01.015.

[40] W. Xu, et al., Increasing coenzyme Q10 yield from *Rhodopseudomonas palustris* by expressing rate-limiting enzymes and blocking carotenoid and hopanoid pathways, Lett. Appl. Microbiol. 73 (2021) 88–95, https://doi.org/10.1111/lam.13479.

[41] W. Cheng, W. Li, Structural insights into ubiquinone biosynthesis in membranes, Science 343 (2014) 878–881, https://doi.org/10.1126/science.1246774.

[42] S. Ren, et al., Structural and functional insights into an archaeal lipid synthase, Cell Rep. 33 (2020), 108294, https://doi.org/10.1016/j.celrep.2020.108294.

[43] S.M. Marques, et al., Web-based tools for computational enzyme design, Curr. Opin. Struct. Biol. 69 (2021) 19–34, https://doi.org/10.1016/j.sbi.2021.01.010.

[44] M. Bilal, et al., State-of-the-art protein engineering approaches using biological macromolecules: a review from immobilization to implementation view point, Int. J. Biol. Macromol. 108 (2018) 893–901, https://doi.org/10.1016/j.ijbiomac.2017.10.182.

[45] H. Jochens, U.T. Bornscheuer, Natural diversity to guide focused directed evolution, ChemBioChem 11 (2010) 1861–1866, https://doi.org/10.1002/cbic.201000284.

[46] X. Li, et al., Computational enzyme design approaches with significant biological outcomes: progress and challenges, Comput. Struct. Biotechnol. J. 2 (2012), e201209007, https://doi.org/10.5936/csbj.201209007.

[47] R. Ramadoss, et al., Substantiation of propitious "Enzybiotic" from two novel bacteriophages isolated from a wastewater treatment plant in Qatar, Sci. Re.p 12 (2022) 9093, https://doi.org/10.1038/s41598-022-13171-8.

[48] D. Contractor, et al., Structural basis of Omicron immune evasion: a comparative computational study, Comput. Biol. Med. 147 (2022), 105758, https://doi.org/10.1016/j.compbiomed.2022.105758.

[49] J.G. Caporaso, et al., QIIME allows analysis of high-throughput community sequencing data, Nat. Methods 7 (2010) 335–336, https://doi.org/10.1038/nmeth.f.303.

[50] M. Estaki, et al., QIIME 2 enables comprehensive End-to-End analysis of diverse microbiome data and comparative studies with publicly available data, Curr. Protoc. Bioinformatics 70 (2020) e100, https://doi.org/10.1002/cpbi.100.

[51] B.J. Callahan, et al., DADA2: high-resolution sample inference from Illumina amplicon data, Nat. Methods 13 (2016) 581–583, https://doi.org/10.1038/nmeth.3869.

[52] F. Pedregosa, et al., Scikit-learn: machine learning in python, J. Machine Learn. Res. 12 (2012).

[53] E. Bolyen, et al., Reproducible, interactive, scalable and extensible microbiome data science using QIIME 2, Nat. Biotechnol. 37 (2019) 852–857, https://doi.org/10.1038/s41587-019-0209-9.

[54] E. Pruesse, et al., SILVA: a comprehensive online resource for quality checked and aligned ribosomal RNA sequence data compatible with ARB, Nucleic Acids Res. 35 (2007) 7188–7196, https://doi.org/10.1093/nar/gkm864.

[55] C. Quast, et al., The SILVA ribosomal RNA gene database project: improved data processing and web-based tools, Nucleic Acids Res. 41 (2013) D590–D596, https://doi.org/10.1093/nar/gks1219.

[56] J. Zhang, et al., Improving coenzyme Q10 yield of *Rhodobacter sphaeroides* via modifying redox respiration chain, Biochem. Eng. J. 135 (2018) 98–104, https://doi.org/10.1016/j.bej.2018.04.006.

[57] R.C. Edgar, MUSCLE: multiple sequence alignment with high accuracy and high throughput, Nucleic Acids Res. 32 (2004) 1792–1797, https://doi.org/10.1093/nar/gkh340.

[58] Y. Xue, et al., GPS: a comprehensive www server for phosphorylation sites prediction, Nucleic Acids Res. 33 (2005) W184–W187, https://doi.org/10.1093/nar/gki393.

[59] C. Wang, et al., GPS 5.0: an update on the prediction of kinase-specific phosphorylation sites in proteins, Genomics Proteomics Bioinformatics 18 (2020) 72–80, https://doi.org/10.1016/j.gpb.2020.01.001.

[60] L. Kall, et al., Advantages of combined transmembrane topology and signal peptide prediction–the Phobius web server, Nucleic Acids Res. 35 (2007) W429–W432, https://doi.org/10.1093/nar/gkm256.

[61] U. Omasits, et al., Protter: interactive protein feature visualization and integration with experimental proteomic data, Bioinformatics 30 (2013) 884–886, https://doi.org/10.1093/bioinformatics/btt607.

[62] C. UniProt, UniProt: the universal protein knowledgebase in 2021, Nucleic Acids Res. 49 (2021) D480–D489, https://doi.org/10.1093/nar/gkaa1100.

[63] M. Steinegger, J. Söding, MMseqs2 enables sensitive protein sequence searching for the analysis of massive data sets, Nat. Biotechnol. 35 (2017) 1026–1028, https://doi.org/10.1038/nbt.3988.

[64] T. Bailey, M. Gribskov, Combining evidence using p-values: application to sequence homology searches, Bioinformatics 14 (1998) 48–54, https://doi.org/10.1093/bioinformatics/14.1.48.

[65] T.L. Bailey, et al., The MEME Suite, Nucleic Acids Res. 43 (2015) W39–W49, https://doi.org/10.1093/nar/gkv416.

[66] Yang, J. and Zhang, Y. (2015) I-TASSER server: new development for protein structure and function predictions. *Nucleic Acids Res.* 43, W174–181. 10.1093/nar/gkv342.

[67] J. Yang, et al., The I-TASSER Suite: protein structure and function prediction, Nat. Methods 12 (2015) 7–8, https://doi.org/10.1038/nmeth.3213.

[68] A. Roy, et al., I-TASSER: a unified platform for automated protein structure and function prediction, Nat. Protoc. 5 (2010) 725–738, https://doi.org/10.1038/nprot.2010.5.

[69] R. Laskowski, et al., PROCHECK: a program to check the stereochemical quality of protein structures, J. Appl. Crystallogr. 26 (1993) 283–291, https://doi.org/10.1107/S0021889892009944.

[70] M. Wiederstein, M.J. Sippl, ProSA-web: interactive web service for the recognition of errors in three-dimensional structures of proteins, Nucleic Acids Res. 35 (2007) W407–W410, https://doi.org/10.1093/nar/gkm290.
[71] E.F. Pettersen, et al., UCSF Chimera—A visualization system for exploratory research and analysis, J. Comput. Chem. 25 (2004) 1605–1612, https://doi.org/10.1002/jcc.20084.
[72] C.M. Labbe, et al., MTiOpenScreen: a web server for structure-based virtual screening, Nucleic Acids Res. 43 (2015) W448–W454, https://doi.org/10.1093/nar/gkv306.
[73] S. Yuan, et al., Using PyMOL as a platform for computational drug design, WIREs Comp. Mol. Sci. 7 (2017), https://doi.org/10.1002/wcms.1298.
[74] R.A. Laskowski, et al., PDBsum: a web-based database of summaries and analyses of all PDB structures, Trends Biochem. Sci. 22 (1997) 488–490, https://doi.org/10.1016/S0968-0004(97)01140-7.
[75] R.A. Laskowski, PDBsum: summaries and analyses of PDB structures, Nucleic Acids Res. 29 (2001) 221–222, https://doi.org/10.1093/nar/29.1.221.
[76] R.A. Laskowski, PDBsum new things, Nucleic Acids Res. 37 (2009) D355–D359, https://doi.org/10.1093/nar/gkn860.
[77] A. Legat, et al., Identification of polyhydroxyalkanoates in Halococcus and other haloarchaeal species, Appl. Microbiol. Biotechnol. 87 (2010) 1119–1127, https://doi.org/10.1007/s00253-010-2611-6.
[78] R. Mahansaria, et al., Polymerase chain reaction-based screening method applicable universally to environmental haloarchaea and halobacteria for identifying polyhydroxyalkanoate producers among them, Extremophiles 19 (2015) 1041–1054, https://doi.org/10.1007/s00792-015-0775-9.
[79] P. Greenspan, et al., Nile red: a selective fluorescent stain for intracellular lipid droplets, J. Cell Biol. 100 (1985) 965–973, https://doi.org/10.1083/jcb.100.3.965.
[80] C. Ospina-Betancourth, et al., Enhancement of PHA Production by a Mixed Microbial Culture Using VFA Obtained from the Fermentation of Wastewater from Yeast Industry, Fermentation 8 (2022), https://doi.org/10.3390/fermentation8040180.
[81] D. Inoue, et al., Polyhydroxyalkanoate production potential of heterotrophic bacteria in activated sludge, J. Biosci Bioeng. 121 (2016) 47–51, https://doi.org/10.1016/j.jbiosc.2015.04.022.
[82] M. Akdoğan, E. Çelik, Purification and characterization of polyhydroxyalkanoate (PHA) from a *Bacillus megaterium* strain using various dehydration techniques, J. Chem. Technol. Biotechnol. 93 (2018) 2292–2298.
[83] M. Li, et al., Characteristics and application of *Rhodopseudomonas palustris* as a microbial cell factory, Front. Bioeng. Biotechnol. 10 (2022), 897003, https://doi.org/10.3389/fbioe.2022.897003.
[84] S.Q. Lee, et al., Cellular factories for coenzyme Q10 production, Microb. Cell Fact 16 (2017) 39, https://doi.org/10.1186/s12934-017-0646-4.
[85] X. Robert, P. Gouet, Deciphering key features in protein structures with the new ENDscript server, Nucleic Acids Res. 42 (2014) W320–W324, https://doi.org/10.1093/nar/gku316.
[86] C. Zardecki, et al., RCSB protein data bank: a resource for chemical, biochemical, and structural explorations of large and small biomolecules, J. Chem. Educ. 93 (2016) 569–575, https://doi.org/10.1021/acs.jchemed.5b00404.
[87] H. Huang, et al., Structure of a membrane-embedded prenyltransferase homologous to UBIAD1, PLoS Biol. 12 (2014), e1001911, https://doi.org/10.1371/journal.pbio.1001911.
[88] R. Pearce, Y. Zhang, Deep learning techniques have significantly impacted protein structure prediction and protein design, Curr. Opin. Struct. Biol. 68 (2021) 194–207, https://doi.org/10.1016/j.sbi.2021.01.007.
[89] K.E. Kemege, et al., *Ab initio* structural modeling of and experimental validation for *chlamydia trachomatis* protein CT296 reveal structural similarity to Fe(II) 2-oxoglutarate-dependent enzymes, J. Bacteriol. 193 (2011) 6517–6528, https://doi.org/10.1128/JB.05488-11.
[90] J. Jumper, et al., Highly accurate protein structure prediction with AlphaFold, Nature 596 (2021) 583–589, https://doi.org/10.1038/s41586-021-03819-2.
[91] L. Wessjohann, B. Sontag, Prenylation of Benzoic Acid Derivatives Catalyzed by a Transferase from Escherichia coli Overproduction: method Development and Substrate Specificity, Angewandte Chemie Int. Edition in English 35 (1996) 1697–1699, https://doi.org/10.1002/anie.199616971.
[92] C.H.M. Rodrigues, et al., DynaMut2: assessing changes in stability and flexibility upon single and multiple point missense mutations, Protein Sci. 30 (2021) 60–69, https://doi.org/10.1002/pro.3942.
[93] S. Jiang, et al., *Stappia albiluteola* sp. nov., isolated from marine sediment, Int. J. Syst. Evol. Microbiol. 71 (2021), https://doi.org/10.1099/ijsem.0.004807.
[94] J.R. Han, et al., *Marinobacter salexigens* sp. nov., isolated from marine sediment, Int. J. Syst. Evol. Microbiol. 67 (2017) 4595–4600, https://doi.org/10.1099/ijsem.0.002337.
[95] J. Li, et al., *Sunxiuqinia indica* sp. nov., isolated from deep sea, Int. J. Syst. Evol. Microbiol. 70 (2020) 4186–4192, https://doi.org/10.1099/ijsem.0.004273.
[96] P. Tedesco, et al., Isolation and characterization of strain *exiguobacterium* sp. KRL4, a producer of bioactive secondary metabolites from a Tibetan glacier, Microorganisms 9 (2021), https://doi.org/10.3390/microorganisms9050890.
[97] H.-.W. Yen, C.-.H. Chiu, The influences of aerobic-dark and anaerobic-light cultivation on CoQ10 production by *Rhodobacter sphaeroides* in the submerged fermenter, Enzyme Microb. Technol. 41 (2007) 600–604, https://doi.org/10.1016/j.enzmictec.2007.05.005.
[98] H.W. Yen, T.Y. Shih, Coenzyme Q10 production by *Rhodobacter sphaeroides* in stirred tank and in airlift bioreactor, Bioprocess Biosyst. Eng. 32 (2009) 711–716, https://doi.org/10.1007/s00449-008-0294-5.
[99] J. An, et al., In vitro antioxidant activities of *Rhodobacter sphaeroides* and protective effect on Caco-2 cell line model, Appl. Microbiol. Biotechnol. 103 (2019) 917–927, https://doi.org/10.1007/s00253-018-9497-0.
[100] W. Li, Bringing Bioactive Compounds into Membranes: the UbiA Superfamily of Intramembrane Aromatic Prenyltransferases, Trends Biochem. Sci. 41 (2016) 356–370, https://doi.org/10.1016/j.tibs.2016.01.007.
[101] L.J. Kingsley, M.A. Lill, Substrate tunnels in enzymes: structure–function relationships and computational methodology, Proteins: Structure, Function, and Bioinformatics 83 (2015) 599–611, https://doi.org/10.1002/prot.24772.
[102] F. Vascon, et al., Protein electrostatics: from computational and structural analysis to discovery of functional fingerprints and biotechnological design, Comput. Struct. Biotechnol. J. 18 (2020) 1774–1789, https://doi.org/10.1016/j.csbj.2020.06.029.